Research Requirements Document

Droplet Flame Extinguishment in Microgravity (FLEX)

Research Team Lead:
Forman A. Williams, University of California, San Diego

NASA Research Team Members:
Michael Hicks, NASA Glenn Research Center
Vedha Nayagam, National Center for Space Exploration Research

External Research Team Members:
Mun Y. Choi, Drexel University
Frederick L. Dryer, Princeton University
Benjamin D. Shaw, University of California, Davis

November 4, 2005

Contents

1 Introduction **6**
- 1.1 Current Practices . . . 6
- 1.2 The NASA FPDS-Suppression Program . . . 7

2 Background - Fire Suppression **9**
- 2.1 Flame Extinction . . . 9
- 2.2 Agent Efficacy . . . 11
- 2.3 CO_2 Suppression Studies . . . 12
- 2.4 Summary . . . 13

3 Droplet Combustion for Fire Suppression Research **15**
- 3.1 Flame Radiative Emission and Reabsorption . . . 17
- 3.2 Soot Formation/Destruction . . . 18
- 3.3 Convective Flow Effects . . . 21
- 3.4 Numerical Modeling . . . 23
- 3.5 Species Transport . . . 25
- 3.6 Summary . . . 27

4 Flight Experiment Description **28**
- 4.1 Experiment Objectives . . . 28
- 4.2 Independent Experiment Variables . . . 29
- 4.3 Experimental Diagnostics . . . 30
- 4.4 Science Data End Products . . . 31

5 Flight Experiment Requirements **35**
- 5.1 Experiment Requirements . . . 35
  - 5.1.1 Test Fuels . . . 36
  - 5.1.2 Droplet Deployment and Ignition . . . 37
  - 5.1.3 Initial Pressure . . . 37
  - 5.1.4 Initial Ambient . . . 37
  - 5.1.5 Misc. Ambient Requirements . . . 38
  - 5.1.6 Ambient Flow Conditions . . . 38
  - 5.1.7 Operational Requirements . . . 38
  - 5.1.8 Microgravity Requirements . . . 39
- 5.2 Diagnostic Requirements . . . 39
  - 5.2.1 Droplet Imaging . . . 41
  - 5.2.2 $OH*$ Flame Imaging . . . 41
  - 5.2.3 Secondary Color Flame Imaging . . . 42
  - 5.2.4 Flame Radiation . . . 42
  - 5.2.5 Soot Volume Fraction Measurement . . . 42
  - 5.2.6 Soot/Fiber Temperature . . . 43
  - 5.2.7 Flow Velocity Measurement . . . 43
  - 5.2.8 Ambient Temperature and Pressure Measurement . . . 44
  - 5.2.9 Synchronization . . . 44
- 5.3 Flight Experiment Test Procedures . . . 44
- 5.4 FLEX Test Matrix . . . 45

6 Post-Flight Data Analysis **56**
6.1 Flight Data Analysis Plan . . . 56
6.1.1 Temporal Droplet History . . . 56
6.1.2 Flame Shape and Structure . . . 56
6.1.3 Soot Volume Fraction . . . 57
6.1.4 Flame Radiation . . . 57
6.2 Science Success Criteria . . . 57
6.2.1 Minimal Success . . . 58
6.2.2 Complete Success . . . 58

7 Ground-Based Research Program **60**
7.1 Test Matrix Determination . . . 60
7.2 Complimentary Experiments . . . 60
7.3 Theoretical/Numerical Model Development . . . 61

8 Management Plan **63**

9 Justification for Reduced Gravity **64**

A Previous Microgravity Droplet Combustion Experiments **73**
A.1 Ground-Based Low Gravity Experiments . . . 73
A.2 Fiber Supported Droplet Combustion Experiment (FSDC) . . . 74
A.3 Fiber Supported Droplet Combustion Experiment - 2 (FSDC-2) . . . 74
A.4 Droplet Combustion Experiment (DCE) . . . 74
A.5 Ground-based studies of Soot Formation/Destruction . . . 75
A.6 Ground-based studies of Soret Diffusion . . . 77
A.7 Summary . . . 81

List of Figures

1 S-shaped curve with flame temperature as a function of Damköhler number. The upper branch (red) is the burning branch and the lower branch (blue) is the non-burning branch. The area between the two turning points (dashed blue) is the unstable regime. 10

2 A conceptual flammability map for a single droplet burning in an infinite ambient. The red curve represents the extinction caused by 'blowoff' of the flame (Law, 1975), while the blue curve represents the radiative extinction branch (Chao et al., 1990). The LOI is the lowest oxygen concentration which will support combustion. 11

3 Data from the DCE reported in Nayagam et al. (1998). The figure demonstrates the two different extinction modes, diffusive extinction for the small droplet and radiative extinction for the large droplet. 17

4 Calculated mass of soot vs. the square of the initial droplet diameter for n-heptane droplets burning in microgravity conditions. 19

5 Radiative heat loss fraction, $\mathcal{X}_r$, normalized by the value at the initial droplet diameter ($1.8\,mm$) as a function of droplet diameter. 20

6 Effect of force convection on methanol droplet burning in microgravity (Dietrich et al., 1996). 22

7 Estimated influences of the oxygen Lewis number (Le_O) on the flame temperature (T_f) of an alkane droplet with various diluent gases. 25

8 Estimated influences of the oxygen Lewis number (Le_O) on the flame temperature (T_f) of an alkane droplet with various diluent gases. 26

9 Laser backlit images for ethanol droplets burning at 2.4 atmospheres and 30% oxygen concentration in a) He b) N_2 c) Ar. 75

10 Ethanol droplets burning in O_2 /N_2 of a) 30%/70% and b) 40%/60% and an ambient pressure of 2.4 atm. 77

11 Heptane droplets burning in air at pressures of a) 1 atm, b) 0.75 atm, c) 0.5 atm, d) and 0.25 atm. 78

12 Images from Shaw (2005) for reduced-gravity combustion of decane/hexadecane droplets with different inert gases. 79

13 Data from Shaw (2005): (a) normalized droplet diameter histories; and (b) flame standoff ratios. 80

List of Tables

1 Reduced Damkohler numbers for various flow configurations 10
2 Gaseous fire suppression agent efficacy, as measured by the MEC , for cup burner flames (Takahashi et al., 2004). 12
3 Science Data End Products. 33
4 Hardware requirements tabulation. 35
5 Diagnostic requirements tabulation. 40
6 Quiescent environment LOI test matrix. 46
7 Slow flow LOI test matrix 47
8 CO_2 suppressant efficacy test matrix. 48
9 He suppressant efficacy test matrix. 50
10 SF_6 suppressant efficacy test matrix. 52
11 Suppressant efficacy in a slow flow test matrix. 54
12 Suppressant in a radiative environment test matrix. 55
13 Residence time (τ_{res}) and flame temperature (T_f) for ethanol droplets burning in ambients with different diluent gases and an oxygen mole fraction of 0.30. 76
14 Gas-phase oxygen transport data for different inert species in a 0.21 oxygen mole fraction ambient. 80

1 Introduction

NASA's new space exploration vision calls for extending a human presence into space beyond low Earth orbit, returning to the Moon, and then to Mars and beyond. Achieving these goals will require many technological advances in life support, environmental monitoring, space suits for extravehicular activity, power generation and storage, food production, and waste management, to name a few. Because a rapid return to Earth is not an option on long duration missions outside of low-Earth orbit, the crew must have the equipment, systems, and procedures to safely deal with both prompt-effect and delayed-effect hazards. Prompt-effect hazards are those requiring an immediate and effective response for alleviation and include fire, atmospheric contamination, injury, explosion, loss of pressure, and meteoroid and debris penetration. Delayed-effect hazards are those requiring less urgent or timely response and include atmospheric contamination, hidden damage, and corrosion.

Fire is a significant prompt-effect hazard, but it also contributes to the delayed-effect hazards through atmospheric contamination, and spacecraft damage. Hence, NASA's fire-protection strategies must cover a wide range of areas from the control and suppression of the fire to the restoration, repair, and cleanup activities after a fire event. The first line of defense in a Fire Safety policy is fire prevention through material selection and control. Experience in manned space flight, however, demonstrates that this control is not sufficient to prevent fires on spacecraft. Therefore, fire detection and suppression systems are required in the event a fire does occur. Our understanding of the processes involved in microgravity fire suppression, particularly with regard to the practical technology for fire extinguishment, is very limited. In general, fire suppression in microgravity has only been investigated in small-scale experiments using relatively simple geometries.

1.1 Current Practices

The Shuttle and International Space Station (ISS) both have portable fire extinguishers for use by the crew. Carbon dioxide is the current fire suppressant in the U.S. modules and its use is planned for the upcoming Japanese and ESA modules of the ISS. The Russian modules use hand-held water-based foam extinguishers, similar to those used on the *Mir* Orbiting Station.

Opfell (1985) and Panzarella and Lewis (1990) performed trade studies to evaluate potential suppressants before the selection of CO_2 as the fire suppressant on the ISS. The criteria they used to evaluate various agents and techniques included:

1. The effectiveness against potential fires;
2. The reliability of the agent;
3. The maintainability of the suppressant system (especially important for long duration missions);
4. The weight of the system (up-mass considerations);
5. The procedures and materials required for post-fire cleanup;
6. The toxicity of the suppressant by itself and any by-products of its interaction with the fire;
7. Any collateral damage caused by use of the suppressant.

Therefore, while the effectiveness of a suppressant to extinguish a fire is important, it is not the sole factor in determining an appropriate choice. The overall goal of the suppression element of the

Fire Prevention, Detection and Suppression (FPDS) program at NASA is to evaluate candidate suppressants in light of the factors listed above.

The fire suppression techniques currently employed for spacecraft, however, are based almost entirely on testing and practices in normal gravity. The reduced and microgravity environment aboard spacecraft creates fire scenarios that are dramatically different than those on earth. For example, flammability limits of a given material in reduced gravity environment can be dramatically different in microgravity than in normal gravity, and in fact, it is possible to have a flammability reversal[1] (T'ien, 1990). In the absence of gravity, the distribution of a suppressant is very different not only for condensed phase suppressants, but also for gaseous ones because of the lack of buoyant convection.

As a result, fire suppression is much different in reduced gravity than in normal gravity, not only because of the difference in the fires, but also because of the dispersal of the suppressant. Therefore, NASA has developed a fire safety program that deals specifically with the fire suppression in reduced gravity. The program consists of programs and individuals in academia, NASA, and other agencies including NIST, the agency responsible for fire suppression standards in the United States.

1.2 The NASA FPDS-Suppression Program

The suppression of a real fire, whether it is in normal or reduced gravity environments, involves a complex interaction of a range of physical and chemical phenomena. As such, there is no ideal single experiment or model which can be considered the 'gold standard' to determine an agent's effectiveness with respect to the three criteria above. A 'first-principle' model of a real fire is computationally prohibitive assuming all of the relevant physics are known in sufficient detail. Full-scale experiments are expensive and there is no way to test all of the possible fire scenarios. Therefore, a comprehensive fire suppression program will cover a wide range of topics ranging from fundamental to practical fire studies. The fundamental studies will provide data and models from which researchers derive verified sub-models that are elements of realistic fire scenarios.

The FPDS program, with the assistance of microgravity combustion PIs and NASA researchers, developed three primary objectives (essentially a subset of the objectives above) for the suppression portion sub-topic. These are:

i. Determine suppressant effectiveness in reduced gravity

ii. Characterize large-scale agent deployment in reduced-gravity

iii. Verify suppressant system design rules through reduced-gravity testing of relevant fuels and/or geometries

The fire suppression program based at the NASA Glenn Research Center is a comprehensive program designed specifically to address fire suppression in reduced-gravity environments with respect to the criteria above.

The major difference between the two environments is in the buoyancy-driven flow present in normal gravity fires. This flow dominates the species and energy transport in normal gravity fires and also influences suppressant transport to and away from the flame zone. In reduced gravity, convective flows are likely due to ventilation systems (or the suppressant system) where the typical flows are an order of magnitude smaller than those caused by buoyancy in normal gravity fires. Thus, transport processes such as molecular diffusion, particle thermophoresis and radiation become

[1] In this case a given material that is less flammable relative to another in normal gravity will be more flammable than that other material in microgravity

more important and in some cases dominant. Further, gravity dependent phenomena such as fuel dripping (for condensed phase fuels), or settling of liquid-phase suppressants are not present in microgravity. Therefore, while familiarity with normal gravity fire suppression literature is important, the microgravity fire suppression plan must take into account the unique environment present in spacecraft.

One hypothesis that runs through the design of the fire suppression system and the fire response procedures is that steady flame spread on a solid fuel does not occur in a quiescent environment; hence the requirement to cease the ventilation flow upon annunciation of a fire alarm. This is based entirely from fire suppression in normal gravity and predicted performance in microgravity. Movement of the crew, however, during the response and discharge of a fire extinguisher will induce flow velocities also on the order of several cm/s. Olson et al. (1988) have shown that flammability limits for a solid in a $5\,cm/s$ convective flow can be broader in microgravity than in normal gravity where buoyant velocities are greater than $10\,cm/s$ even for a small flame. Recent simulations by Wu and Ruff (2003) have shown that even in the rear volumes of an instrument rack, the discharge of a PFE can produce velocities on the order of $50\,cm/s$ during the initial portion of discharge in spite of the dense packing of equipment[2]. Therefore, the question remains as to how induced velocities will affect the suppressant concentration required to extinguish a fire in reduced gravity.

[2]The velocity is much higher in the vicinity of the CO_2 discharge.

2 Background - Fire Suppression

Fire suppression in human-crewed spacecraft is a complex and multidisciplinary issue. Recent reviews (Friedman, 1998, 1999; Friedman and Urban, 2000; Friedman and Ross, 2001) highlight the issues and review the history, status and future of the important issues. These reviews emphasize that there exist two fundamentally different suppressant application strategies. One of these methods, streaming agent application, requires a concentrated jet of suppressant directed at a particular spot in the fire. The effectiveness of this type of agent application is a strong function of the type of fire and specifics of the extinguishing system.

The second, total agent flooding application, involves essentially diluting the oxidizer with the suppressant to some critical concentration. Quantifying the efficacy of a total flooding agent is ideally suited to study in small, 'bench-scale', systems. These smaller scale systems are less configuration dependent and more suited to detailed modeling. There is, however, no single ideal geometry with which to quantify suppressant efficacy in a flooding application. Fundamentally, however, the suppression of a flame is a flame extinction process and it is therefore worthwhile to review the fundamentals of diffusion flame extinction.

2.1 Flame Extinction

Diffusion flames extinguish when there is insufficient time for chemical reactions to proceed within the narrow flame zone where fuel and oxidizer mix. This reduction in chemical time compared to residence time in a diffusion flame can be brought about by increasing the flow velocity, heat loss from the flame zone thereby reducing the flame temperature, or by limiting the supply of fuel and oxidizer to the flame front. The different physical processes that lead to the ultimate extinguishment of a flame can be viewed in a unified frame-work with the use of a Damköhler number, defined as the ratio of a residence time to a chemical time (Williams, 1974). Fendell (1972) was the first to show that an S-shaped curve is obtained when the flame temperature is plotted against a Damköhler number for a steady diffusion flame (see, Fig. 1). The lower and upper turning points of this S-curve were identified as the ignition and extinction conditions.

Linan (1974) formalized the diffusion flame extinction process using activation energy asymptotic analysis and derived explicit criteria for extinction for a counterflow configuration. Liñán's theory was subsequently extended to various combustion systems, including spherically symmetric droplet combustion (Law, 1975), stagnation point boundary-layer flames of a forced convective flow Krishnamurthy et al. (1976), natural convective burning of a spherical particle (Wu et al., 1982), and flow generated by a spinning fuel disk (Nayagam and Williams, 2000). In all these studies the different flow configuration was recast into the form originally developed by Liñán so that the extinction condition derived by him can be used.

Liñán's analysis relates a reduced Damköhler number at extinction to the environmental conditions surrounding the diffusion flame sheet.

$$\delta_e = \frac{\tau_{ch}}{\tau_r} = f(1 - |\gamma|) \tag{1}$$

where $\gamma = 1 - \frac{2(1-\beta)}{(1+Y_{O\infty})}$, and $\beta = L + \left(\tilde{T}_\infty - \tilde{T}_w\right)$. Here $\tilde{T}_\infty$ is the non-dimensional oxidizer stream temperature, $\tilde{T}_w$ is the non-dimensional fuel stream temperature, and $Y_{O\infty}$ is the oxidizer mass fraction in the ambient. Though the exact form of the reduced Damköhler number changes for different flow configurations, it is still a ratio of a chemical time and a residence time. Table 1 shows a list of reduced Damköhler numbers (Wu et al., 1982) obtained using activation energy

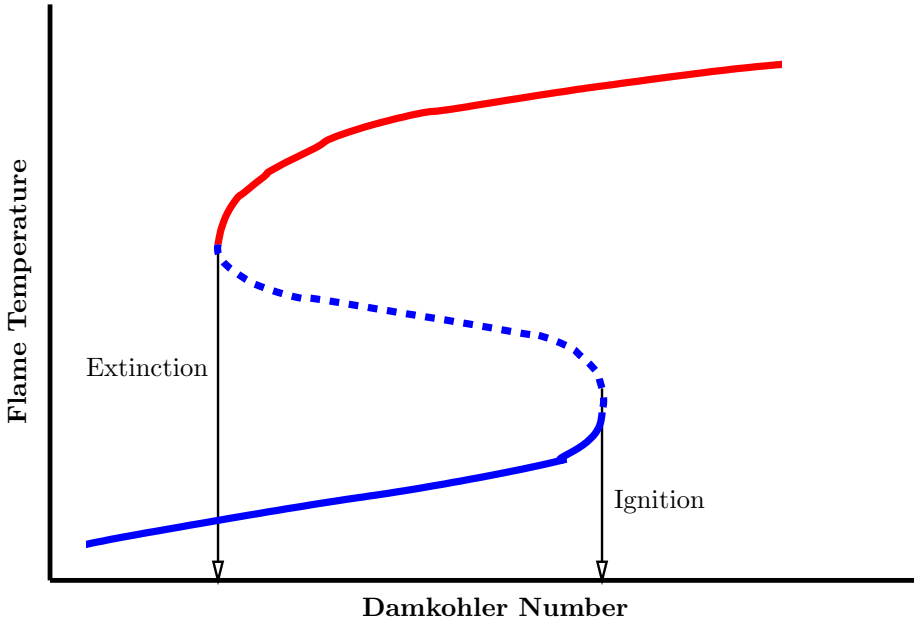

Figure 1: S-shaped curve with flame temperature as a function of Damköhler number. The upper branch (red) is the burning branch and the lower branch (blue) is the non-burning branch. The area between the two turning points (dashed blue) is the unstable regime.

asymptotic models to calculate the extinction condition for diffusion flames embedded in different flow configurations.

Table 1: Reduced Damkohler numbers for various flow configurations

Reduced Damkohler Number (δ)	**Flow Configuration**
$\left[\frac{\ln(1+B)D_{ext}}{(\ln(1+Y_{O\infty}))^2}\right]^2 \frac{C_p}{4M_F}\left(\frac{T_f^2}{T_a}\right)^3 \exp\left(-\frac{T_a}{T_f}\right)$	Droplet Combustion (Law, 1975)
$\left[\frac{(1+B)}{(1+Y_{O\infty})F_N}\right]^2 \sqrt{\frac{D_{ext}}{g}}\left(\frac{K\,\rho}{M_F}\right)\left(\frac{T_f^2}{T_a}\right)^3 \exp\left(-\frac{T_a}{T_f}\right)$	Stagnation-point boundary layer (Wu et al., 1982)
$\left[\frac{(1+B)}{H_w \exp^{h_f}}\right]^2 \frac{4\,\rho\,A_0}{M_F\,c\,Pr\,(1+Y_{O\infty})^2}\left(\frac{T_f^2}{T_a}\right)^3 \exp\left(-\frac{T_a}{T_f}\right)$	Rotating disk stagnation point and von Karman flow (Nayagam and Williams, 2000)

2.2 Agent Efficacy

The expressions for the Damköhler number provide a convenient theoretical basis for flame extinction. Unfortunately, they are not easily used by engineers designing suppression systems or evaluating material flammability issues. For a given material and ambient condition (pressure, diluent type), there exists an oxygen mole fraction below which a steady flame cannot exist. This oxygen concentration is called the Limiting Oxygen Index (LOI). Using the droplet as a model geometry, Figure 2 shows a hypothetical quasi-steady flammability map. The graph shows oxygen concentration on the ordinate and droplet diameter on the abscissa. The curve is essentially the critical Damköhler number and the region inside the curve is flammable and outside the region is non-flammable. The red branch of the curve is the extinction branch defined by Law (1975) and the blue branch is the radiative quench branch defined by Chao et al. (1990). A typical droplet combustion experiment starts by igniting a droplet at a point inside the curve (denoted by the green circle). The droplet then burns until it reaches the red curve where the flame will extinguish. The limiting oxygen index (LOI) is the point where the two curves meet, or the minimum oxygen concentration that will support a quasi-steady flame.

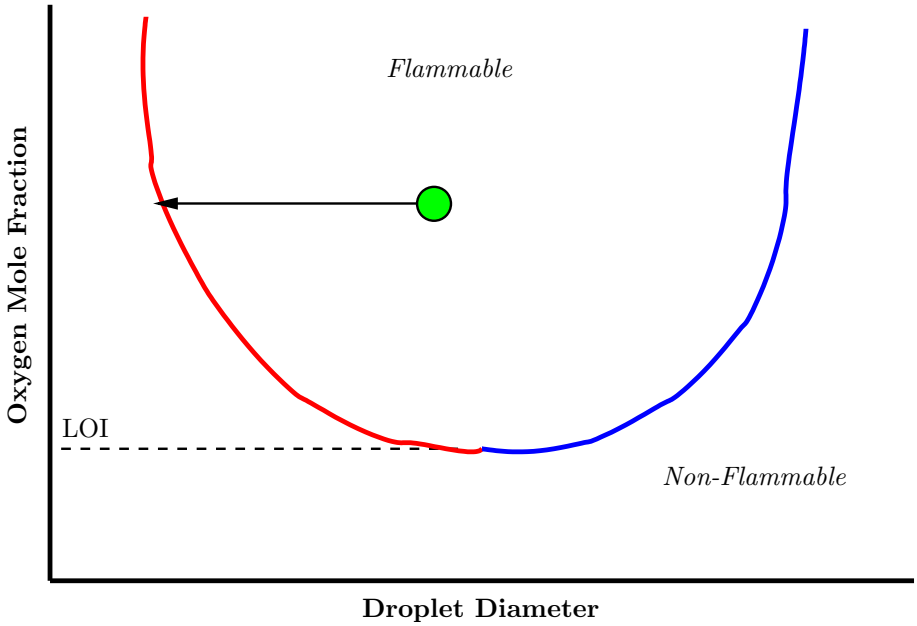

Figure 2: A conceptual flammability map for a single droplet burning in an infinite ambient. The red curve represents the extinction caused by 'blowoff' of the flame (Law, 1975), while the blue curve represents the radiative extinction branch (Chao et al., 1990). The LOI is the lowest oxygen concentration which will support combustion.

The LOI is a critical concept in fire safety, and also important in developing, refining and ultimately validating detailed chemical kinetic mechanisms. For fire safety, the goal of the agent in a total flooding application is to reduce the oxygen concentration below the LOI .

The concepts of extinction and LOI reviewed above define the framework from which to develop a quantitative measure of suppressant agent efficacy. The LOI is often recast in terms of the Minimum Extinction Concentration (the minimum concentration of a suppressant agent above which a quasi-steady flame cannot exist, MEC). The MEC is related to the LOI by the following relationship.

Table 2: Gaseous fire suppression agent efficacy, as measured by the MEC , for cup burner flames (Takahashi et al., 2004).

Agent/Env.	MEC , $1-g$	MEC , μg
CO_2	0.16	0.19
He	0.27	0.31
N_2	0.26	0.38

$$LOI = 0.209\,(1 - MEC) \tag{2}$$

The MEC is a function of the fuel, agent and experimental geometry. Clearly, a more effective agent will have a lower MEC for a given fuel and fuel geometry.

Takahashi et al. (2004) conducted normal gravity tests and microgravity simulations of the suppression of methane cup-burner flames using mixtures of various suppressants in standard air. The table below summarizes the findings for MEC in the two environments.

2.3 CO_2 Suppression Studies

The United States module of the ISS uses CO_2 as the suppressant. The effectiveness of CO_2 as a fire suppressant in a microgravity environment has been studied in the past by several authors (Honda and Ronney, 1998; Katta et al., 2004). Honda and Ronney (1998) studied opposed-flow flame spread rates over thin solid fuels in microgravity by adding different inert diluents (He , N_2 , Ar, CO_2 and SF_6) to the standard air atmosphere. Their experimental results seem to suggest that CO_2 is less effective as a fire suppressant in microgravity than He in terms of the minimum O_2 concentration that supports combustion. Katta et al. (2004) investigated the mechanism through which CO_2 causes fire suppression using detailed numerical simulation and experiments in microgravity for a methane-air diffusion flame stabilized on a cup burner. Their results showed that a CO_2 volume fraction greater than 19.1% is needed to destabilize the flame-base in microgravity compared to 16.4% for a normal gravity flame. They also pointed out the importance of gas-phase radiation in determining extinguishment limits in microgravity.

Radiative thermal losses from the flame zone in reduced gravity environments may be significantly altered when the surrounding gas phase is thermally participating. In most small scale terrestrial fires, when compared with the quenching effects associated with strong buoyantly driven convective flows, radiative quenching plays a relatively minor role in the extinguishment of fires. In these situations the heated gases are quickly lifted from the reaction zone and, as a consequence, quickly cool and provide little radiative feedback to the fuel source.

In the absence of buoyantly-driven convective flows, however, radiative losses from the flame can become a significant fraction of the total heat loss from the reaction zone. When radiative exchanges between the flame and the ambient are limited by the presence of a thermally participating gas, such as CO_2 , temperatures in the proximity of the fuel source will increase. Chernovsky et al. (2005) demonstrated this in a recent set of experiments where fuel side temperature increases were reported in an ethylene (C_2H_2) diffusion flame, using a porous spherical burner, in atmospheres of varying concentrations of CO_2 (20% to 40%).

This radiative feedback effect from the gas phase has been of increasing concern because of the implications in the selection and evaluation of appropriate fire suppressants. The use of CO_2 , an

optically thick gas in the infrared region of the electromagnetic spectrum, has garnered widespread acceptance as an effective fire suppressant for most ground based applications. Since buoyant forces typically dominate the flow field in 1-g environments the temperature field between the flame front and the fuel surface is not significantly affected by radiative absorption and re-emission in the surrounding gas phase. Once surrounding gas temperatures increase, buoyant forces will induce flows that cause the heated gases to be swept away from the reaction zone. However, in reduced gravity environments, where buoyant forces are negligible, heated gases will have a longer residence time in the reaction zone and the effects of gas phase radiation on the thermal feedback to the fuel surface as well as on the reaction rates, which are affected by elevation in the localized temperature field, become important in the assessment of the performance of different fire suppressants.

The radiative feedback effects of CO_2 , as well as other potential fire suppressants, have been largely un-quantified in the selection and ranking of fire suppressants for spacecraft fires. Since the extinction mechanism of many microgravity flames is radiation-dominated the emissive and absorptive properties of the surrounding gases will play a significant role in the extinction process. Reuther (1985) mentioned this radiative interplay between flame and surroundings in discussing the ranking criteria of fire suppressants. He reasoned, however, that CO_2 should be ranked the highest. The paper stated:

> *"For a suppressant to be effective radiatively, it must decrease flame luminosity, act as a radiation sink itself, and remain transparent between the flame and its surroundings. On this basis CO_2 was favored because CO_2 decreases sooting in diffusion flames by 20% to 30% more than does N_2 and CO_2 is more active radiatively (infrared) than N_2 ."* Reuther (1985)

It is not entirely clear, however, that CO_2 is 'transparent' in the distances, temperatures, and concentrations that may come into play in the event of a release in the International Space Station or in future extra-terrestrial applications with lunar and/or martian gravity levels. Additionally, it is not clear that consideration was made of the possibility that radiative emissions from the heated gases, following a substantial fire, could potentially serve more as a radiative 'source' rather than a radiative 'sink'.

2.4 Summary

A suppressant agent in an oxidizing gas can influence a diffusion flame in a number of ways; it can alter the diffusion rates of fuel and oxidizer to the flame front, the conductive heat losses from the flame, the flame temperature through its thermal capacity when the flame is not quasi-steady, altering the chemical kinetic mechanisms, and the net radiative energy loss. All of these have the net effect of reducing the Damköhler number below a critical value. The Damköhler number provides a framework through which fire suppressant effectiveness can be studied in different flame geometries, and their results related to one another (Williams, 1974). Hamins et al. (1994) has shown that such similarities exist between counter-flow diffusion flames and cup-burner flames in ranking suppression effectiveness.

A judiciously selected, chemically inert gas could be used as a fire suppressant in human space exploration missions with minimal physiological impact, unlike chemically active agents that may produce harmful combustion byproducts. At present CO_2 is used as a fire suppressant in the United States Module of the International Space Station. CO_2 is not physiologically inert at the concentrations necessary to extinguish fires in microgravity. In addition, because CO_2 is radiatively participating and not removed by buoyant convection, it's effectiveness in microgravity as a fire suppressant merits further investigation.

In summary then, there is clearly a need for studies in simplified geometries that lend themselves to detailed study both experimentally and theoretically/numerically to evaluate the effectiveness of gaseous suppression agents. Droplet combustion experiments in microgravity provide a simple configuration to investigate the effectiveness of chemically inert suppressants.

The droplet geometry is not typical typical of those which have been used previously for fire safety studies, but it is ideal in many aspects. First, the geometry lends itself to detailed analytical and computational modeling (one dimensional). These experimental data used in conjunction with these models will lead to verified detailed and reduced models which can be used directly in models of more realistic fires. Second, the flame interacts with a condensed phase, an aspect found in almost all practical fires (in normal or microgravity), although in this case the properties of the condensed phase are very well known. Third, length and time scales are easy to vary (through changes in droplet diameter). In fact, during a single test a droplet will continually change length and timescales, moving from regimes of stable burning to unstable burning (in some cases) to non-flammable regimes (for cases where the flame extinguishes at a finite droplet diameter). Finally, the physical phenomena identified as important in determining droplet burning and flame extinction are known to be important in practical fire suppression including finite rate chemical kinetics, soot production, transport and destruction, radiant energy loss and reabsorption, species transport effects, etc.

3 Droplet Combustion for Fire Suppression Research

The spherically symmetrical combustion of a liquid fuel droplet in a quiescent ambient gaseous oxidizing atmosphere is a classical problem in combustion research, having been addressed first more than 50 years ago by Godsave (1952), Hall and Diederichsen (1953) and Spalding (1952, 1953). Numerous reviews of the subject are now available in the literature, among them those of Wise and Agoston (1958), Williams, F. (1956), Williams (1973),Faeth (1977), Law (1982), Sirignano (1993, 1999), Avedisian (2000), Chiu (2000) and Choi and Dryer (2001). An advantage of the spherical symmetry is that only one space dimension enters the description of the combustion process, so that one-dimensional (spherically-symmetrical) time-dependent conservation equations apply, greatly facilitating both computational and theoretical descriptions of the combustion and thereby enhancing understanding of experimental results, which becomes much more difficult, uncertain and inaccurate in multidimensional situations. Natural convection, however, destroys the spherical symmetry of the combustion in normal gravity, as was quite evident in the earliest experiments of Hall and Diederichsen (1953) and Goldsmith (1956). **?** was the first to realize that microgravity experiments afforded the opportunity to achieve spherical symmetry, a fact of which NASA has taken advantage in fundamental investigations for a number of years (Williams, 1981; Dietrich et al., 1996; Nayagam et al., 1998). Although microgravity experiments are, in a sense, somewhat artificial for earthbound combustion, they are of direct concern for combustion hazards in the spacecraft which are needed to pursue human exploration of planets and their satellites in space.

Fire safety in spacecraft must be addressed broadly, from both fundamental and applied viewpoints, if space habitats are to be made as safe and secure as possible, and this necessitates paying attention to the combustion behaviors of all types of fuels that may be present, in all of the various configurations that these fuels may be found, both in the presence and absence of fire-suppression activities. Because the relative simplicity of droplet combustion leads to better understanding of experimental results and thereby promotes improving evaluations of what combustion phenomena may occur in more complex configurations, studies of microgravity droplet combustion in oxidizing atmospheres continuing different amounts of diluents and fire suppressants can contribute fundamental information that will be useful in assessing fire safety. It is relevant to review the combustion aspects of droplets that are shared by other fuels, both liquid and solid, in other configurations.

One fundamental way to characterize different materials is in terms of their elemental chemical constituents. Polyethylene, for example, is a hydrocarbon, while polyformaldehyde and cellulose, for example, contain oxygen as well, while other materials contain other elements. The preponderance of combustible materials in space-flight applications are of the first two types, namely containing only carbon and hydrogen or containing carbon, hydrogen and oxygen. While different materials behave quite differently in the condensed phase during combustion, their gas-phase behaviors subsequent to gasification often better reflect their elemental composition. For example, hydrocarbons are more prone to gas-phase soot formation during combustion, while oxygenated materials tend to produce less soot, and soot is known to affect combustion phenomena (Choi et al., 1990; Manzello et al., 2001). Since heptane is a hydrocarbon while methanol is oxygenated, some differences in combustion behaviors of different materials can be simulated in droplet-burning investigations of these two different liquid fuels.

Radiant energy transfer is known to be important in fires, and different burning materials in different configurations will experience different effects of radiant energy transfer. The same is true in droplet burning, in which radiant energy loss from the flame to the surroundings as well as radiant energy feedback from the flame to the condensed-phase fuel both may be important. Sufficiently large heptane droplets, for example, have been observed to exhibit radiative extinction

(Nayagam et al., 1998; Ackerman et al., 2003) and a similar phenomenon is known in the combustion of methanol droplets as well (Dietrich et al., 1996; Marchese and Dryer, 1996a; Zhang and Williams, 1997, 1998). Studies of droplet combustion thus can help in sorting out effects of radiant energy transfer in combustion and fire suppression and in clarifying the relationships between soot production and radiant energy emissions.

In flames near extinction, there is, in general, a competition between radiant energy loss and conductive energy loss (Chao et al., 1990). At large dimensions radiant energy losses tend to dominate, while at smaller sizes conductive losses dominate. In studies of fire safety and suppression, the LOI is important, and for safety reasons it is desirable to know the smallest value of the LOI for a combustible material, in both oxygen-nitrogen mixtures and in mixtures of air with gaseous fires suppressants other than nitrogen (for example, CO_2). This information determines, for example, the amount of a suppressant that is needed to be sure to extinguish a fire. In complex configurations it can be difficult to determine the minimum value of the LOI because of the large number of different geometrical dimensions that need to be varied. Microgravity studies of droplet combustion offer the great advantage of having only one geometrical dimension, the droplet diameter. As the droplet diameter is varied, there is a transition from conduction-dominated losses at small diameters to radiation-dominated losses at large diameters, there thus being a critical droplet diameter exhibiting the minimum LOI . Moreover, there are indications that the minimum LOI values found in droplet-burning experiments are lower than those of other experiments (Dryer, personal communication), so that the droplet-burning results will be conservative in the sense that atmospheres below this minimum LOI are unlikely to support combustion in any configuration. Experiments on LOI in microgravity droplet combustion therefore are very important for assessing spacecraft fire safety.

Convective phenomena also influence combustion and fire suppression, both in bringing oxygen to the fuel more efficiently and in transporting fire suppressants to the flame. Droplet-combustion experiments with small imposed convective velocities can help in ascertaining such convective effects for all types of burning materials in microgravity because the gas-phase convection is independent of the condensed-phase fuel type. Convection affects both the tradeoff between conductive and radiative energy transfer and the sooting characteristics, for example by influencing gas-phase fuel-rich residence times. Depending on conditions, variable convection can either enhance combustion or inhibit it. Better knowledge of convection effects therefore would be helpful in determining combustion behavior and effective fire suppression. As the relative convective velocity between gas and a burning material is increased, a velocity is reached at which combustion is extinguished (Wu et al., 1982), and determination of such extinction velocities for droplet combustion is relevant to fire suppression. There thus is motivation for looking not only at droplet combustion in various quiescent atmospheres but also at combustion and extinction in those atmospheres with controlled imposed convection. Unlike earthbound fires, where natural convection is dominant, in spacecraft only forced convection is present, and its effects can be quite different from those commonly experienced on Earth.

In summary then, studies of microgravity droplet combustion in different atmospheres can benefit strategies for fire suppression in space habitats for a number of reasons. One is the well-defined relevant geometrical parameter, the droplet diameter, that can be varied systematically to achieve different combustion regimes. Another is the facility with which minimum LOI and convective extinction velocities can be obtained. A third is the ability to distinguish behaviors of different classes of materials on the basis of their elemental compositions. And finally, by accurately controlling the atmospheric pressure and composition, relative influences of different suppressants can be quantified. In view of these many advantages, the FLEX program seems likely to exert favorable influences on fire safety in human space exploration.

3.1 Flame Radiative Emission and Reabsorption

Microgravity droplet combustion experiments (e.g., Nayagam et al., 1998) have clearly demonstrated two distinct extinction modes. Diffusive extinction of a droplet flame occurs when the characteristic time of flow of reactants through a given distance becomes shorter than the time required for energy release through chemical reactions in that same distance. This relationship is defined by the Damköhler number which is a non-dimensional ratio of the characteristic flow time (due to diffusive transport) to the characteristic chemical reaction time. Diffusive extinction can be superseded by radiative extinction for large droplets. Radiative extinction in droplet combustion occurs when significant reduction in temperature is caused by radiative losses within the reaction zone (Chao et al., 1990).

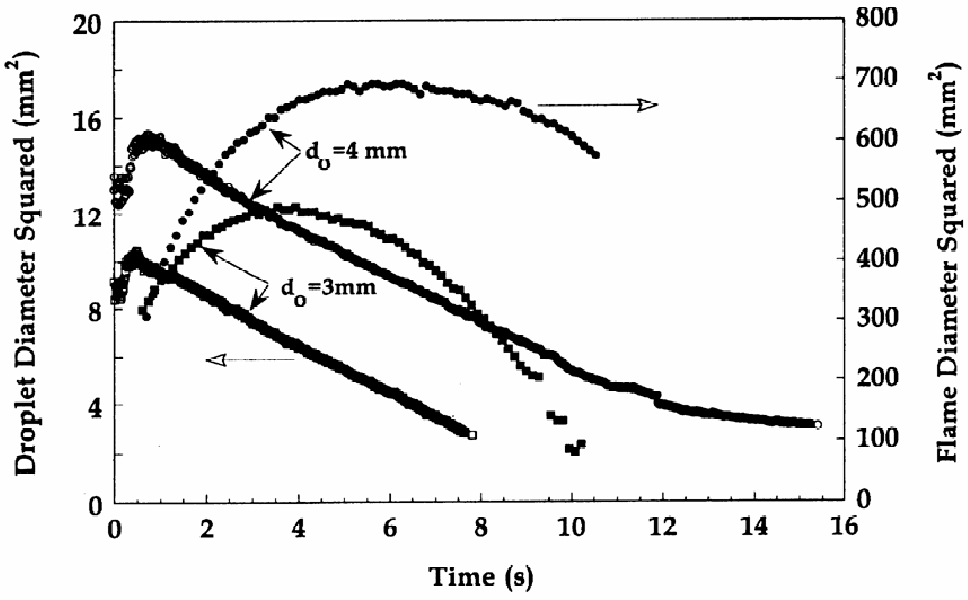

Figure 3: Data from the DCE reported in Nayagam et al. (1998). The figure demonstrates the two different extinction modes, diffusive extinction for the small droplet and radiative extinction for the large droplet.

Nayagam et al. (1998) investigated the diffusive and radiative extinction phenomena by varying the initial droplet size and the oxygen concentration (with helium as the inert). Figure 3 displays the square of the flame and droplet diameters as a function of time for two separate experiments using different initial droplet diameters burning in 30% O_2 /70% He . The larger droplet flame extinction is strongly influenced by radiative losses, whereas the smaller droplet flame extinction results almost solely from diffusive effects. The distinction between the two is illustrated in the occurrence of extinction relative to the fractional burning time. Radiant energy loss from the flame structure is proportional to the cube of the flame radius, and increases, as the flame produced at ignition moves outward and fuel accumulation effects occur. At large flame radii, the variation of diffusive terms with flame radius is small in comparison to those for radiative loss, and although

diffusive effects remain, the radiative decrease of the flame temperature dominates the extinction process. In Figure 3, the flame of the larger droplet (4 mm diameter) is extinguished at a flame diameter that is within approximately 10% of the maximum flame diameter, whereas the flame of the smaller droplet (3 mm) extinguishes at a much later time which nearly corresponds to complete burnout.

In these experiments, significant soot formation was observed in the backlit views. Therefore, in order to completely understand the importance and magnitude of the radiative loss, it is important to understand in detail the soot formation/destruction during droplet burning.

3.2 Soot Formation/Destruction

As a 'real' spacecraft material burns in microgravity, the radiative heat loading, oxygen deprivation, and view obscuration from the fire-generated particulates may present a greater danger to the crew than the flame itself. Therefore, it is paramount that the flame suppression studies include fuels that form soot to accurately represent conditions that are to be expected in an actual fire in microgravity conditions. A droplet burning in a microgravity offers a unique environment for studying soot formation/destruction processes in detail because conditions can be varied from non-sooting cases to heavily-sooting cases by merely controlling the initial droplet size, ambient pressure, oxygen concentrations, convection, and inert substitution as parameters.

In 1990, Choi et al. (1990) reported that the burning rates of n-heptane droplets under microgravity conditions were strongly influenced by the formation of soot particles. The formation of soot through pyrolysis reactions (pyrolysis reactions are strongly endothermic) serves as a heat sink, which will reduce the effective heat of combustion and therefore the transfer number. Reductions in the burning rate constant are expected for conditions of significant soot conversion, even though the transfer number appears in the natural log term of the classical expression. Related to these phenomena is the accumulation of the formed soot into a spherical sootshell. The accumulated (and trapped) soot represents material for which chemical energy release will not be realized. The relative importance of these soot-related mechanisms is dependent on the magnitude of soot concentration within the droplet flame.

In 1996, Choi and Lee (1996) performed the measurements of soot concentrations for n-heptane droplet flames burning in microgravity conditions. These experiments revealed that under buoyancy-free environments, significant soot concentrations (with a maximum as high as 60 ppm) are produced even for a fuel that was considered to be lightly sooting based on observations made under normal-gravity conditions. Figure 4 displays the calculated soot mass plotted as a function of square of the droplet diameter which can be used to ascertain the relationship between sooting propensity and the droplet dimension (Lee et al., 1998). In these experiments, (Lee et al., 1998) demonstrated that the sooting propensity increases with initial droplet size while the mean droplet burning rate decreases with initial droplet size.

Based on these measurements, Lee et al. (1998) estimated the relative importance of the radiative heat loss due to soot by considering the radiative heat loss fraction, $\mathcal{X}_r$. $\mathcal{X}_r$ is the ratio of radiative power, Q_r, divided by rate of heat generation, Q_c. The radiative power for sooting diffusion flames can be formulated as (Hall, 1988)

$$Q_r = \int_{r_s}^{r_f} 4\pi C \, f_v \, T^5 \, r^2 \, dr \tag{3}$$

where $C = 2.97x10^{-11} \, W/\left(cm^3 \, K^5\right)$, f_v is the soot volume fraction and r_s and r_f are the droplet and flame radii, respectively. Q_r can be calculated using measured soot volume fraction distributions (Choi and Lee, 1996) and predicted temperature distributions using a detailed numerical

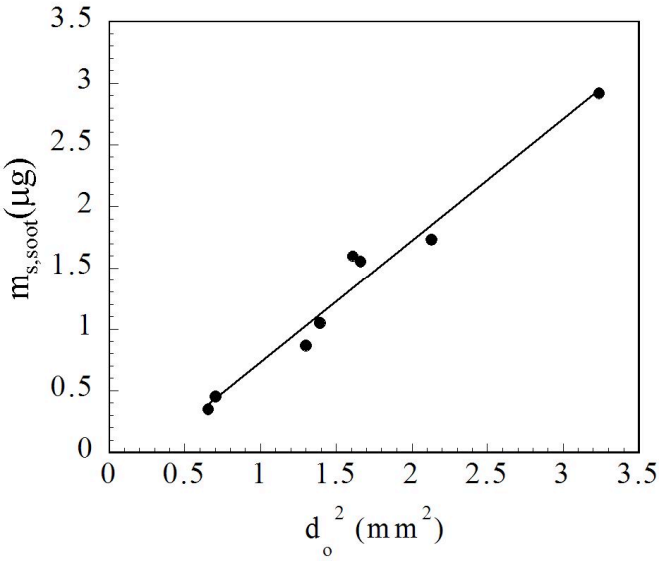

Figure 4: Calculated mass of soot vs. the square of the initial droplet diameter for n-heptane droplets burning in microgravity conditions.

model inclusive of non-luminous radiation effects (Marchese and Dryer, 1997a). The rate of heat generation, $\mathcal{Q}_c = \dot{m}\mathcal{H}$, was calculated as the product of the heat of combustion and the rate of mass consumption (computed from the instantaneous burning rate constant). Figure 5 displays $\mathcal{X}_r$ as a function of initial droplet diameter for the present experiment. The strong influence of initial droplet diameter on the radiative heat loss fraction is clearly evident. The radiative heat loss fraction will be dependent on the chosen temperature distribution and its variation with initial droplet diameter. Nonetheless, the trend of increasing radiative heat loss fraction for larger droplets that is determined in the present study (based on measured soot volume fraction and predicted temperature distributions and burning rates) is supported by radiometric measurements performed by Colantonio and Nayagam (1997) for n-heptane combustion under microgravity conditions. Their measurements indicated that the fraction of radiant energy to the heat release increases with initial droplet size.

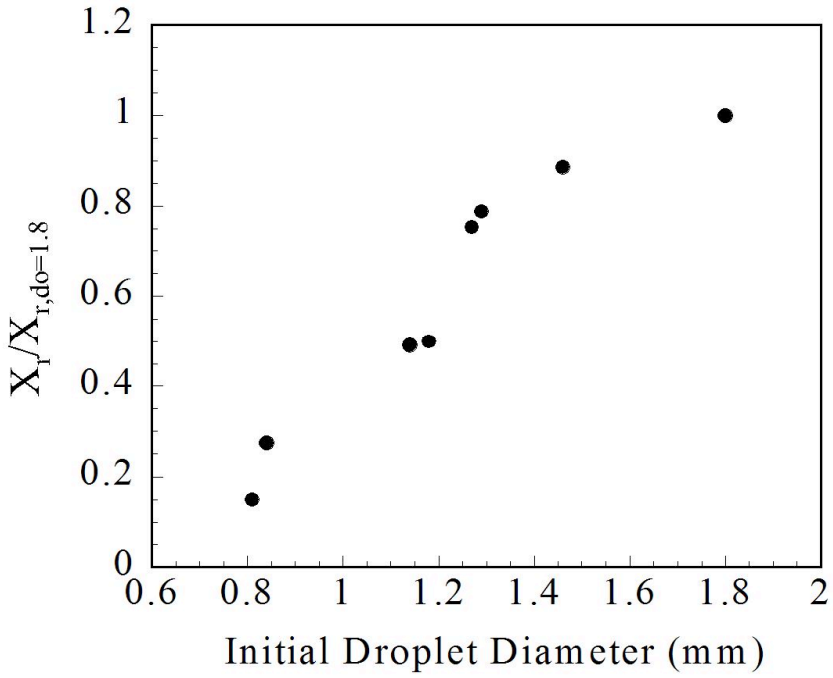

Figure 5: Radiative heat loss fraction, $\mathcal{X}_r$, normalized by the value at the initial droplet diameter (1.8 mm) as a function of droplet diameter.

It has also been observed in subsequent microgravity investigations that radiant loss rates associated with sooting should decrease with increasing dilution and decreasing pressure (Williams, 2001). Furthermore, efforts to investigate forced convection (created by the various methods of flame suppression) on sooting and radiative heat losses will require examination of the changes in the residence times required for soot formation and growth. Recent experiments in ground-based facility have demonstrated a strong influence of convection on sooting behavior for microgravity droplet flames (Nayagam et al., 2003).

The importance of soot formation in diffusion flames is summarized in a 2003 report by the National Academy of Engineering (NAP, 2003) which stated that "formation and oxidation of soot particles are intimately tied to their temperature, which is affected by radiation. This means that

studies of radiation cannot be decoupled from those of soot formation and oxidation." Because of its likely presence in real fires and its importance in determining flame structure and extinction limits, soot must be an integral part of any fire suppression study. Optimally, this should be studied in a geometrically simple arrangement which lends itself to detailed study, both experimentally and theoretically/numerically. As part of the fire safety study using the FLEX platform, baseline cases and the resulting influences of sooting and radiative heat losses caused by oxygen variation, inert substitution, reduced-pressure, and inert and chemically-active suppressant flow on n-heptane microgravity droplet flames will be investigated.

3.3 Convective Flow Effects

Under normal Earth gravity environment the density differences caused by heat release at the flame-zone generates buoyancy-induced flows unlike in a microgravity environment onboard spacecrafts. Sub-buoyant convective flows, however, are always present within a spacecraft due to ventilation and air-conditioning system operation. Furthermore, as indicated previously, in the event of a fire, application of fire-suppressant to the flaming region or depressurization of the cabin could also lead to slow convective flows depending on the fire suppressant application technique and the rate of depressurization. Therefore, it is important to understand the effects of slow convection on the flammability and extinction boundaries of condensed fuels with and without the presence of suppressants.

Slow convection around a burning fuel droplet alters the burning and extinction processes in many ways by its nonlinear interaction with other competing phenomena, such as radiation, conductive or diffusive heat loss from the flame-zone, and soot formation. It is also well known that flames surrounding condensed fuels can be sustained by slow moving oxidizer flow under conditions that can not support burning in normal gravity or quiescent microgravity environments. A practical implication of this behavior, as pointed out by T'ien (1990), is the possibility of flammability ranking reversal for a material from normal gravity to microgravity. The LOI for condensed fuels depends both on the ambient oxygen concentration and the flow velocity.

There are only a few experimental studies where the effects of forced convection on burning and extinction of droplet flames have been considered. Okajima and Kumagai (1974, 1982) were the first to report experimental results for fuel droplets burning in a slow convective flow in microgravity. Imposed forced flow velocities varied from zero to 45 cm/s, the initial droplet diameters from 1 to 2 mm with heptane, benzene, and ethanol fuels. Envelope flames were observed for heptane burning in air at atmospheric pressure below an imposed velocity of 45 cm/s. Gokalp et al. (1988) reported observations of n-heptane droplets burning in a forced convective flow under normal gravity and in microgravity (parabolic flights on board KC-135 aircraft). A limited number of convective droplet experiments were conducted using the Glovebox facility in the Spacelab during the USML-2 and MSL-1 space shuttle flights (Dietrich et al., 1996; Nayagam et al., 1998). Figure 6 shows the effect of forced convection on methanol droplet burning in microgravity. The droplet burns in quiescent ambient during the first 8 seconds followed by forced convective burning. The forced convective flow was imposed by turning on the fan. The measured values of burning rate constants for single heptane droplet burning in air when used in the FrÖssling -type correlation yield a value of 0.4 for $\bar{k}$ which is somewhat higher than Okajima and Kumagai results but similar to the observations of Gokalp and co-workers. The ratio of the downstream flame length to upstream flame standoff distance was a constant (1.6) which is somewhat smaller than the value obtained by Okajima and Kumagai for a higher flow velocity. These studies were primarily interested in the quasi-steady burning characteristics of fuel droplets and did not consider the LOI or the suppressant effectiveness.

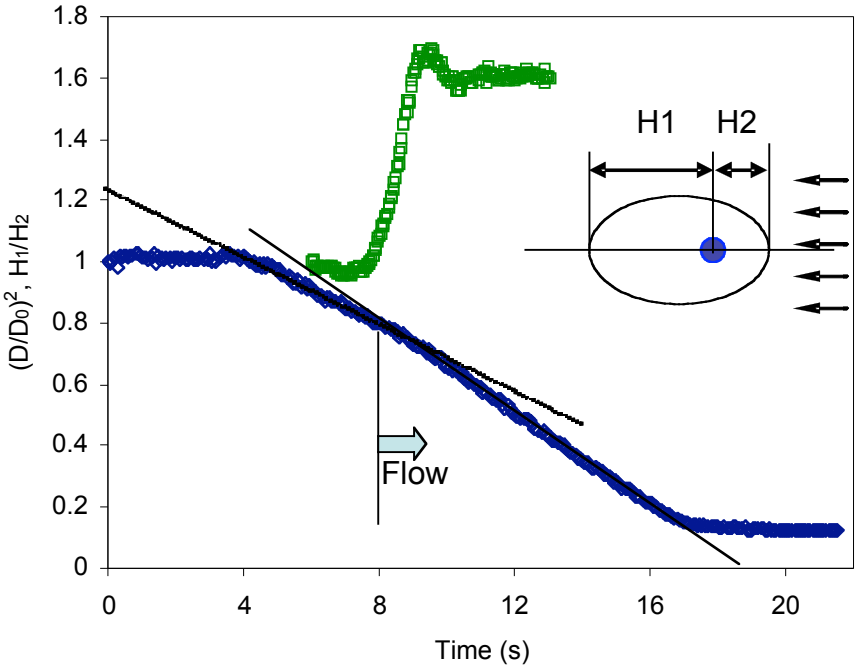

Figure 6: Effect of force convection on methanol droplet burning in microgravity (Dietrich et al., 1996).

There are also only a few theoretical treatments of slow convective droplet combustion. Fendell and co-workers (Fendell et al., 1966) were the first to investigate the effects of forced convection on droplet burning using perturbation techniques. Ayyaswamy and co-workers (Gogos et al., 1986; Gogos and Ayyaswamy, 1988; Jog et al., 1996) removed many of the approximations included in Fendells analysis and developed a perturbation solution using Reynolds number as a perturbation parameter. Their analysis predicts that the leading order correction to the burning rate due to convection is linear in Peclet number, i.e.,

$$\dot{m} = \dot{m}_0 \ (1 \ + \ Pe_\infty) \tag{4}$$

where the Peclet number, Pe_∞ is evaluated at the ambient conditions, and k_0 is the burning rate for spherically symmetric droplet combustion. A similar analysis for carbon particle combustion in a slow convective flow has been carried out by Blake and Libby (1991), Blake (2002) and Ackerman and Williams (2005). These theoretical studies do not consider finite rate chemical kinetic effects and thus cannot address flame extinction.

There are several numerical simulations of convective droplet burning are available in the literature (e.g. Dwyer and Sanders, 1986; Pope and Gogos, 2005). Among these, only Pope and Gogos (2005) consider droplet flame extinction in a forced convective flow field. They show that numerically computed (diffusive) extinction conditions can be correlated by plotting an extinction Damköhler number against the Reynolds number as suggested by asymptotic theories (Krishnamurthy et al., 1976; Wu et al., 1982). Their numerical model neglects radiative heat transfer from the flame and is capable of predicting only the diffusive extinction and not the radiative extinction that is observed in slow convective regimes in microgravity.

3.4 Numerical Modeling

The final and key topic of the proposed program is the development of validated, small dimensional chemical kinetic, radiative energy transport and mass transport models for inclusion in large scale fire simulations. In addition to providing interpretive ability for experimental observations, numerical modeling of spherically symmetric isolated droplet combustion is a means of developing, validating, and testing both robust detailed and low dimensional sub-model components for fire safety applications. It is typically computationally prohibitive to include detailed treatment of all relevant physical phenomena in modeling practical fire (and suppressant) behavior. Thus it is important to develop small dimensional submodel components that are physically and chemically realistic that can be successfully used in such computational tools. Predictive tools for the determination of LOI and other fire safety related criteria can be generated with greater success through mathematical analyses of and comparisons with results produced from detailed, validated models that emulate the combustion and extinction behavior of the fuels utilized in this study. The sub-mechanisms required in these models must include chemistry components that yield reasonable predictions of sooting, for both the luminous and non-luminous radiative interactions will impact the fire safety related observations. These chemistry models must be capable of being integrated with transport sub mechanisms for both gaseous and particulate species, nucleation, growth, coagulation, and oxidation of carbon particulates, and both non-luminous and continuum radiation sub-models. The experimental data collected as part of the proposed program provide the experimental observations that permit successful refinement and validation of state of the art numerical models that can predict the observed burning rate, flame structure and extinction behaviors. The uniqueness of spherically symmetric combustion and appropriate coupling with weak convective fields are essential in allowing the both the original detailed and dimensionally reduced sub-model components to be directly compared in terms of computational predictions (Choi and Dryer, 2001).

Since 1990, (Cho et al., 1992), researchers at Princeton University have pursued numerical modeling for predicting the combustion characteristics of isolated liquid fuel droplets of n-heptane (Held et al., 1997; Marchese et al., 1996, 1999b; Nayagam et al., 1998; Manzello et al., 2001; Choi and Dryer, 2001; Kroenlein et al., 2004), methanol (Marchese and Dryer, 1996b; Marchese et al., 1999a), methanol-water (Marchese et al., 1999a), ethanol and ethanol-water (Kazakov et al., 2003; Urban et al., 2004; Yozgatligil et al., 2004a,b; Li et al., 2005; Mehl et al., 2005), and n-heptane/n-hexadecane mixtures (Marchese and Dryer, 1996a). Ground-based earth gravity and microgravity experiments as well as microgravity experiments on space platforms have been used in developing, improving and validating these models. The kinetics mechanisms for these models have been under constant improvement on the basis of related chemical kinetic research on oxidation and extinction kinetics (e.g., Li et al., 2005, 2004a,b) and to extend the modeling capabilities for alkanes such as n-heptane (Chaos et al., 2005a), n-decane (Zhao et al., 2004, 2005) and n-hexadecane (Chaos et al., 2005b). The droplet combustion model also includes sub-model component implementations for representing dissolution and revaporization of combustion products and liquid-phase additives (Marchese and Dryer, 1996a; Kazakov et al., 2003; Mehl et al., 2005), and internal liquid phase transport enhancement from solutal and thermal Marangoni effects (Marchese and Dryer, 1997b; Kroenlein et al., 2005), as well as low gas/drop convection, non-luminous radiative coupling (Lee et al., 1997). Continuing efforts are developing refined, reduced models for internal liquid phase transport characteristics (Kroenlein et al., 2005), coupling detailed combustion kinetic models with sooting sub-mechanisms, soot nucleation, growth, coagulation, and oxidation sub-model components (Mehl et al., 2005), and including axi-symmetric low gas/drop convection effects on droplet burning and extinction processes. While the prior works under the DCE and SEDC programs have been directed toward advancing the fundamental science issues related to energy conservation of and emissions from conventional and alternative liquid fuels, the same fundamental modeling aspects are essential to developing robust, detailed predictive models for fire safety related parameters. Central to the present proposed program is the integration of the sub model components discussed in other sections into numerical tools that can provide means of validating sub-model components against the generated experimental data, and a test-bed for developing and demonstrating low dimensional representations of these sub-models.

Another effort at the University of California, Davis involves development of a multidimensional computational model focusing on fiber influences on droplet vaporization. The code is based on overset grid technology and presently uses three grids to model a droplet on a fiber. There is an overall major grid, which is cylindrical in shape. This grid extends to the boundaries of the computational/physical space. A minor grid is fit to the droplet and the third grid is fit to the fiber. This model, which includes detailed transport, heat transport along the fiber and solutal and thermal Marangoni flows, can model vaporization of a fiber-supported droplet. Future enhancements will include ability to model combustion of a fiber-supported droplet.

The code has been used for the following studies, which involve mass transfer without combustion: (1) the influence of fiber size on droplet and gas flow physics; (2) the influence of fiber size on surface tension driven flows; (3) the influence of fiber heating on the droplet mass transfer distribution; and (4) mass transfer with surface tension influences and droplet heating at high pressure and droplet cooling at low pressure. In all cases the surface tension forces are dominant. In addition, a parametric study has been carried out on the influence of gas pressure and droplet size on surface tension forces and mass transfer. Dwyer et al. (2004) and Shringi et al. (2005) summarize the results of the results of these studies.

3.5 Species Transport

The low dimensional models that result from the detailed models will invariably involve simplified transport models for species and energy. Global species transport in normal gravity fires is generally dominated by rapid buoyant convection. Convective flow velocities on a spacecraft in reduced gravity, however, are typically much smaller ($\sim\ 10^{-2}\ 10^{-1}\ m/s$). These velocities are typical of ventilation flows, suppressant flows and crew movement. Diffusive transport, including Soret diffusion[3], is therefore much more important (especially with a suppressant agent in the gas). Even if buoyant flows are prevalent, e.g., in normal gravity, diffusive transport can be important over small length scales within the preheat and reaction zones.

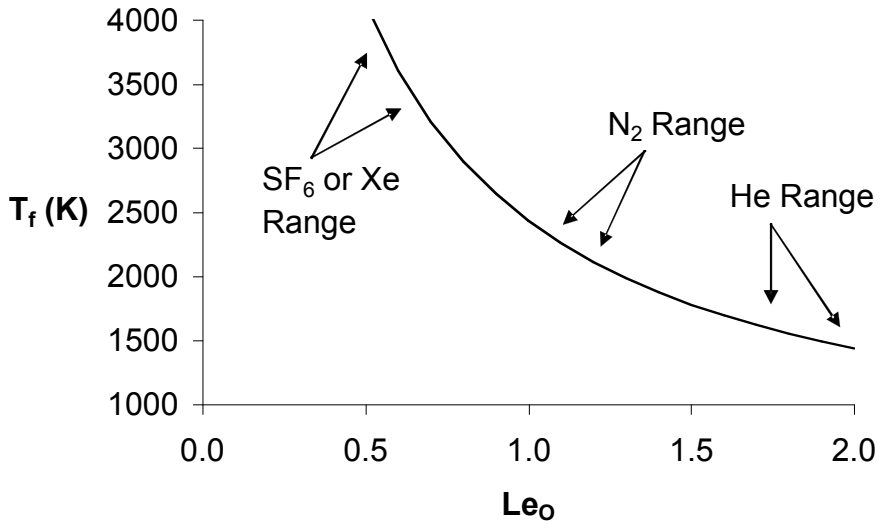

Figure 7: Estimated influences of the oxygen Lewis number (Le_O) on the flame temperature (T_f) of an alkane droplet with various diluent gases.

Soret transport, i.e., species diffusion caused by temperature gradients, can be significant if large differences in molecular weight or size exist between the diluent and other species (e.g., oxygen or fuel). Traditional wisdom stated that consideration of Soret transport is important only when modeling light species such as H and H_2 (Warnatz et al., 1996). This viewpoint, however, does not account for the possibility that one or more species in a mixture could be much heavier or different in size than the other species present, potentially leading to significant Soret transport effects related to transport of heavy fuel species (or their pyrolysis products) to an oxidation zone. Rosner et al. (2000) stressed that Soret effects should be accounted for when calculating diffusive transport of heavy species. In related work, Dakhlia et al. (2002) showed (computationally) that

[3]Other transport effects such as pressure-gradient diffusion and the Dufour effect may also be present in reacting gas mixtures. These effects, however, are generally quite small under combustion situations (even when the Soret effect is not), and as such they are not described further here.

Soret transport decreases flame temperatures by as much as 125 K when He is used as a diluent in a counterflow spray diffusion flame (compared to using N_2). They found that Soret transport strongly affected streamwise and the species field around vaporizing fuel droplets. Williams (2001) also emphasized the importance of including accurate molecular transport models, including models of Soret transport, when calculating extinction conditions for nonpremixed counterflow flames.

Soret transport can also influence transport of O_2 to droplet flame zones (Aharon and Shaw, 1998). Kassoy and Williams (1968); Law (1982); Cheatham and Matalon (1996); Mills and Matalon (1998) showed that droplet combustion characteristics can depend significantly on the oxygen Lewis number, Le_O, between the environment and the flame. Because radiant heat loss and flame extinction characteristics depend primarily on the flame temperature, it is important to understand influences of Le_O as much as possible. Figure 8 shows estimates of the flame temperature (T_f) as a function of Le_O for a heptane droplet burning in an environment with an ambient oxygen mass fraction of 0.23. These estimates, developed using simplified theory advanced by Law (1982), assume complete combustion and constant properties. Even with these assumptions, it is clear that variations in the Le_O can have a strong effect on the flame temperature. $Le_O \approx 0.5$ corresponds to using SF_6 or Xe as a diluent, leading to the hottest flames, while $Le_O \approx 2$ (and perhaps larger) corresponds to using He as a diluent and produces the coolest flames. The case $Le_O \approx 1$ is for when N_2 is the diluent and produces an intermediate flame temperature.

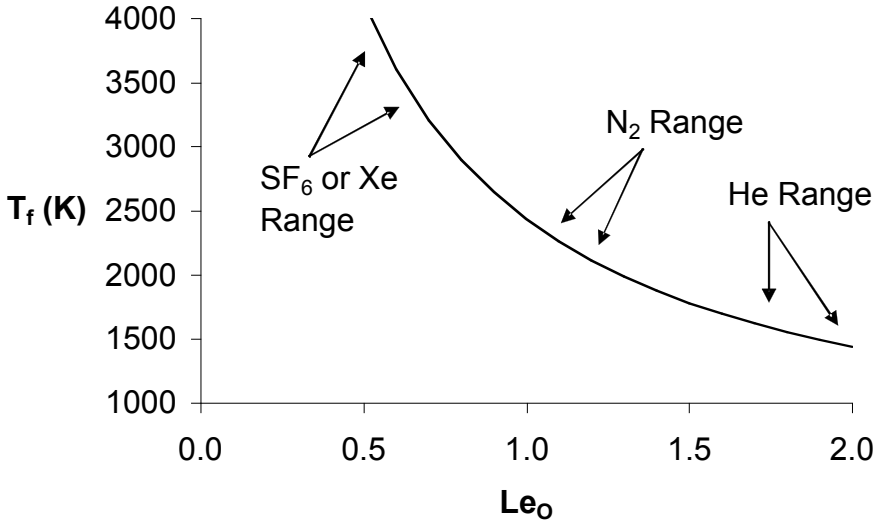

Figure 8: Estimated influences of the oxygen Lewis number (Le_O) on the flame temperature (T_f) of an alkane droplet with various diluent gases.

Previous space-based experiments with large ($\approx 5mm$) alkane droplets in air showed that flames for large droplets can be very dim (Dietrich et al., 1996; Shaw et al., 2001). When a high molecular weight species such as SF6 is present in the gas phase, it is likely that Soret-enhanced transport of O_2 to the flame zone will increase flame temperatures and decrease flame sizes, leading to differences in

combustion and extinction behaviors. In order to develop accurate models to predict such behaviors under conditions where experimental data do not exist, e.g., a multidimensional fire situation, it is important to increase understanding of diffusive transport effects as much as possible so that simplifications may be introduced in a rational fashion without compromising solution accuracy, allowing more complex flow fields to be simulated.

A component of the proposed FLEX research program will examine diffusive transport in detail with the goal of validating and improving diffusive transport models for use in theoretical and numerical simulations of droplet combustion. Particular emphases will be to examine the influences of Soret transport and multicomponent diffusion effects on transport of species to and from flame zones, e.g., through appropriate modeling of Lewis numbers, with the resulting influences on transient combustion behaviors (e.g., burning rates and flame standoff ratios), radiant heat transfer, extinction, and sooting.

3.6 Summary

The combustion and extinction characteristics of liquid fuel droplets in microgravity are determined by the complex interaction of fuel vapor and oxidizer transport, fuel vaporization, conductive, convective and radiative heat loss and chemical kinetics. All of these phenomena are critical in real fire scenarios and thus in understanding the complex issues involved in the design of an effective fire suppression system. The simplicity of the droplet geometry lends itself to detailed theoretical and numerical studies. By comparing the results of the experiments to these detailed treatments it is possible, with today's computational resources, to develop validated chemical kinetic and heat and mass transport mechanisms for liquid fuels. From these fundamental mechanisms it becomes possible to develop validated, predictive, reduced-scale mechanisms that are appropriate for modeling real fire suppression scenarios aboard future spacecraft. The FLEX program, when integrated with the rest of the ground-based and possible flight fire suppression program will yield both a quantitative measure of the effectiveness of various suppression agents and more importantly a set of predictive tools that will allow the effective, efficient design of future spacecraft fire suppression systems.

From a practical perspective, the droplet geometry is again ideally suited for fire suppression studies aboard ISS. With the burning droplet, it is relatively easy to construct the diagram in Fig. 2. For solid fuel studies, construction of this diagram typically requires many tests to determine the branches of the curve, essentially iterating between the flammable and non-flammable regions to define a single point on the curve. The droplet, however, intrinsically moves from the flammable region to the non-flammable region which means that each test defines a point on the curve[4] Furthermore, the design of the droplet combustion insert in the CIR allows for the conduct of a large range of droplet combustion experiments, orders of magnitude more than in solid surface experiments. This allows validation of physical and chemical kinetic mechanisms over a much larger range of ambient conditions, thus improving the predictive capability of the detailed and reduced mechanisms.

The following sections detail the objectives and requirements of the space-based FLEX experiment. There will also be a comprehensive ground-based program that is briefly described in a subsequent section.

[4]Determination of the radiative quench branch using the droplet geometry still requires an iterative approach.

4 Flight Experiment Description

The flight experiment utilizes the spherically symmetric combustion of a fuel droplet in a quiescent ambient as a model geometry to study, on a fundamental level, the relative efficacy of fire suppression agents in microgravity. This section provides an overview of the flight experiment and includes a detailed description of the specific test objectives, the independent experiment variables, the diagnostic requirements and the specific experiment deliverables.

4.1 Experiment Objectives

The proposed project utilizes the spherically-symmetric geometry of droplet combustion as a model environment for quantifying the efficacy of gaseous suppressants. The first and main element of the project is a space experiment that will provide detailed experimental data over a range of independent variables relevant to fire suppression. The second element uses the data from the experiment to develop, refine and validate predictive numerical codes. These codes will in turn be used to develop sub-models of chemistry, radiation and transport for inclusion in more practical models of fire suppression. The third element of the proposed project is a comprehensive ground-based program that includes normal and reduced gravity testing to refine and optimize the test matrix for space experiment, and also to obtain benchmark droplet combustion data at a small subset (smaller length and time scales) of the relevant environments. The specific objectives of the program (flight and ground-based) are:

1. Map the flammability boundaries for liquid fuel combustion in reduced gravity.

2. Quantify the suppressant efficacy of various gaseous suppressants over the range of candidate atmospheric pressures and O_2 concentrations.

3. Develop predictive theoretical/numerical codes and chemical kinetic schemes to model flammability boundaries as a function effective gravitational acceleration on the unique ambient conditions encountered in space exploration applications.

   The development and validation of these model will require detailed spatially and temporally resolved measurements of droplet burning rate, flame extinction, flame radiation, soot concentration, soot temperature, etc.

4. Develop improved and validated reduced (simplified) theoretical/numerical sub-models of important physical processes (chemical kinetics, radiation, soot formation/destruction) that can be used in simulations of large scale, 'realistic' fires.

As stated previously in this document, the droplet geometry is not a practical geometry, but instead is a model geometry where important physical and chemical phenomena can be isolated and studied in detail. The simplicity of the geometry and the nature of the experiment[5] make it an ideal forum to study phenomena important to fire suppression in greater detail than in more practical geometries. This research will focus on several key topics involving droplet combustion with an ambient gas containing a well-mixed, gaseous suppressant.

These experiments will consist of a series of droplet combustion experiments both on the ground and in space to examine fire suppression phenomena in detail. The experiments involve dispensing, deploying and igniting a single droplet in a known and controlled gaseous environment. The

[5] A shrinking, burning droplet moves from a region of stable combustion, potentially through an unstable region, to a non-flammable region in one test

ignited droplet burns to either completion or the flame extinguishes at a finite droplet diameter in a quiescent ambient. The only exception is for a small subset of tests where the droplet is subjected to a known and controlled small, sub-buoyant flow. The primary independent experiment variables are described in the next section, followed by a discussion of the diagnostics. The exact requirements in tabular form for the hardware and diagnostics are discussed in subsequent sections.

4.2 Independent Experiment Variables

Oxygen Mole Fraction: The ambient oxygen mole fraction in a typical space environment can vary from high concentrations in EVA pre-breathing environments down to that typically found in air. At high oxygen concentrations, however, the chemical times are small enough (relative to the characteristic flow times) such that the droplets will burn to completion rather than exhibiting flame extinction. Therefore, it is also necessary to study low oxygen concentrations, down to the LOI. It is also important to determine the LOI in order to verify the chemical mechanisms. The oxygen mole fractions in the present study will vary from 0.10 to 0.50. The chamber must also be large enough such that there is no significant decrease in ambient oxygen mole fraction during an experiment (i.e. the droplet burns in an essentially constant ambient).

Diluent (non-suppressant): The ambient mixture will consist of oxygen mixed with a suppressant and the balance of an inert diluent gas. The diluent gas for these studies will be primarily N_2 since that is the typical diluent on earth and expected in space. There will be a small number of tests with a He diluent gas. The reason is primarily for baseline comparisons with DCE experiments which used He as the diluent gas and also to vary the physical properties of the diluent gas.

Suppressant Type: The tests will examine candidate gaseous suppressants that have widely varying physical, chemical and radiative properties. This will enable model and sub-model development and validation over a wide range of ambient conditions to improve the predictive capabilities of the models. The suppressants are CO_2 , He and SF_6 . The expected concentrations range from 0.00 mole fraction to the limit where no flame can exist (0.70 expected for the least active suppressant).

Pressure: Ambient pressure does not significantly influence the droplet burning rate, but does influence chemistry at sufficiently low values. In addition, one strategy for extinguishing a fire is to isolate the habitat where it exists and vent the cabin to space. It is therefore beneficial to have verified suppressant data at low pressures. The pressure for the tests will range from 0.5 to 1.0 atm. As with the oxygen mole fraction, it is important that the test chamber be sufficiently large so that the pressure is essentially constant during an experiment (i.e. the droplet burns in a constant pressure ambient).

Fuel Type: The advantage of the droplet geometry is that the fuel is relatively simple and better characterized than typical fuels in fire safety studies (e.g. PMMA or paper). This is also a disadvantage since it does not represent a practical fuel. The study will use two typical hydrocarbon fuels, an alcohol, methanol (CH_3OH) and an alkane, heptane (C_7H_{16}). There is a relatively large experience base with these fuels. CH_3OH has a fuel-bound oxygen atom, and burns with a very dim blue flame (not much soot production) with a small standoff distance, so it has widely different radiative characteristics than C_7H_{16} . Therefore, studying these two fuels gives a wide range of fire scenarios to verify model and sub-model performance over.

Droplet Diameter: Figure 2 shows the hypothetical flammability map, and diagrams how a droplet combustion experiment is conducted. The droplet is ignited in the flammable region and then burns in a constant oxygen mole fraction ambient until flame extinction. Under the assumption of quasi-steady burning, the initial droplet size should not significantly influence the determination of the extinction droplet size. Transient influences, however, will be present, so some variation in initial droplet diameter is necessary to determine the deviation from quasi-steady behavior. The initial droplet size in the proposed study will vary between 2 and 5 mm.

4.3 Experimental Diagnostics

The instrumentation for the space-based droplet combustion experiments is based on diagnostics successfully applied to droplet combustion experiments in ground-based facilities. These techniques were selected to provide detailed, quantitative data in addition to qualitative observations of the droplet combustion process. This data can then be used to develop, refine and validate models and reduced sub-models of the relevant physical and chemical phenomena important to spacecraft fire safety.

Droplet Size: The primary diagnostic is a backlit view of the droplet which allows the determination of the droplet size as a function of time. The time evolution of the droplet size yields the droplet burning rate (heat release), and extinction droplet size. It is a critical diagnostic, and the resolution both spatially and temporally must be such that the droplet burning rate (instantaneous as well as average) and droplet extinction diameter may be accurately determined. For the tests where the droplet is supported on a small support fiber, the focal plane of the droplet view must be parallel to the support fiber. The field of view should be sufficient to completely image the droplet during the entire droplet lifetime.

Color Flame Imaging: This view is critical because it provides an overall qualitative view of the burning droplet. This essentially replaces the researchers' eyes and enables the investigators to get an overall view of the combustion process.

$OH*$ Imaging: This view provides both a qualitative and quantitative view of the flame. The $OH*$ better defines the flame than plain video imaging. In addition, color video imaging is typically dominated by visible soot emission (e.g. for C_7H_{16}) and overwhelms chemiluminescence from CH and OH. Therefore, for sooting flames this measurement is necessary to accurately identify the actual flame location. Finally, because the numerical model includes detailed chemistry including OH, it is possible to get better comparison between the experiment and numerical model using the OH image (Marchese et al., 1996).

This view requires sufficient spatial and temporal resolution to accurately capture the time extinction occurs and the flame size and thickness at extinction. The view must also have sufficient dynamic range to capture the flame throughout the burning from immediately after ignition to extinction.

Flame Radiation: Radiative loss is extremely important in microgravity flames. At sufficiently large droplet sizes, radiative energy loss can lead to flame extinction (Chao et al., 1990). Even in conditions where radiative loss is not the prime mechanism for flame extinction (e.g. the red curve in 2), radiative loss is still a significant energy loss mechanism and can influence the extinction droplet size and the determination of the LOI.

Therefore, it is important to quantify the magnitude of the radiative loss. This loss can be spectral losses from species such as CO_2 and H_2O or broadband losses from soot. In order to quantify the magnitude of the radiative loss, it is necessary to measure water vapor radiation and broadband radiation. The water vapor emission measurement must be spectrally filtered ($1.87\,\mu m$) and the broadband measurement sufficiently broad ($0.6 - 5.0\,\mu m$) to adequately characterize the radiative field.

Soot Volume Fraction and Temperature: Soot is important in fire safety for two reasons. First, it is a significant broad band radiator and thus it can influence the burning and extinction characteristics during combustion. Second, soot that escapes the flame zone is a significant long-term health hazard to the crew. Therefore, it is important to understand quantitatively the mechanisms of soot formation and destruction during droplet combustion.

The FLEX investigative team requires the capability to measure both soot volume fraction and soot temperature. These measurements combined with the radiometer measurements will allow for a detailed view of the radiometric emission from a burning droplet. The diagnostic must be able to measure soot volume fractions and temperatures from levels where they constitute a significant fraction of the radiant emission to the maximum levels expected during combustion).

4.4 Science Data End Products

The Science Data Products represent the manner in which the data obtained from testing will be analyzed; the deliverables indicate the information that will ultimately presented and the format in which it will be presented. The deliverables are listed below while the Science Data Products are presented in Table 2.1 on the following page, which provides a summary of the diagnostics necessary to meet the stated science objectives.

1. Map the flammability boundaries for liquid fuel combustion in reduced gravity.
   (a) Determine the extinction droplet diameter as a function of pressure and oxygen concentration for the subject fuels.
   (b) Determine the LOI as a function of pressure for the subject fuels.
   (c) Determine transient effects on the flammability boundary.
2. Quantify the suppressant efficacy of various gaseous suppressants over the range of candidate atmospheric pressures and O_2 concentrations.
   (a) Determine the extinction droplet diameters as a function of pressure and oxygen concentration in the subject suppressants.
   (b) Determine the LOI as a function of the subject suppressant.
   (c) Determine the heat release rate and radiant loss/reabsorption as a function of subject suppressant.
3. Develop predictive theoretical/numerical codes and chemical kinetic schemes to model flammability boundaries as a function effective gravitational acceleration on the unique ambient conditions encountered in space exploration applications.
4. Improved and validated reduced (simplified) theoretical/numerical sub-models of important physical processes (chemical kinetics, radiation, soot formation/destruction) that can be used in simulations of large scale, 'realistic' fires.

(a) Radiation

(b) Chemical kinetic mechanisms including the influence of the suppressant

(c) Soot formation and destruction

(d) Transport, including the influence of Soret diffusion on determining the burning and extinction chararteristics

(e) Small, sub-buoyant convective flows

Table 3: Science Data End Products.

No.	Science Objectives	Diagnostics	Science Data End Product
1a	D_{ext} as a function of oxygen and pressure	- OH flame view with CIR LLL-UV camera - Flame view with MDCA color camera - Back-lit images from CIR HiBMs cameras	- Droplet and flame histories with pre-ignition, ignition, extinction and post-extinction behavior - Soot volume fraction and temperature as a function of suppressant type
1b	LOI as a function of pressure	- OH flame view with CIR LLL-UV camera - Flame view with MDCA color camera - Back-lit images from CIR HiBMs cameras	- Plots of oxygen concentration as a function of droplet diameter
1c	Transient effects on the flammability boundary	- OH flame view with CIR LLL-UV camera - Back-lit images from CIR HiBMs cameras. - Wide and narrow band radiometers	- Droplet, flame and radiometric histories for identical conditions over a range of droplet diameters
2a	LOI as a function of suppressant	- OH flame view with CIR LLL-UV camera. - Flame view with MDCA color camera. - Back-lit images from CIR HiBMs cameras	- LOI as a function of pressure for each suppressant
2b	D_{ext} as a function of suppressant	- Back-lit images from CIR HiBMs cameras. - OH flame view with CIR LLL-UV	- Droplet and flame histories for identical conditions with different suppressants - Soot volume fraction and temperature as a function of suppressant type
2c	Heat release rate and reabsorbtion	- Back-lit images from CIR HiBMs cameras - Wide and narrow band radiometers - Soot volume fraction and temperature measurements	- Heat release, radiant output and reabsorption as a function of suppressant - Soot volume fraction and temperature as a function of suppressant type.

3	Predictive numerical/theoretical models	- All experimental data required for model validation over a wide range of parameters	- Validated numerical and theoretical models of droplet combustion including influences of radiation, finite rate chemical kinetics (w/ suppressants), soot and detailed transport
4a	Reduced radiation sub-model	- Back-lit images from CIR HiBMs camera - Wide and narrow band radiometers	- reduced radiant transport model suitable for inclusion in models of realistic models - Soot volume fraction and temperature as a function of suppressant type
4b	Reduced kinetic models	- Back-lit images from CIR HiBMs camera - OH flame view with CIR LLL-UV	- reduced chemical kinetic models suitable for including the influence of suppressants
4c	Reduced soot models	- Soot volume fraction and temperature - OH flame view with CIR LLL-UV - Wide and narrow band radiometers	- reduced soot models including formation, destruction and radiative loss
4d	Simplified transport models	- Back-lit images from CIR HiBMs camera - OH flame view with CIR LLL-UV	- Simplified transport models that include Soret diffusion
4e	Simplified models for influence of convective flows	- Back-lit images from CIR HiBMs camera - OH flame view with CIR LLL-UV - MDCA color camera - Uses data on freely floated droplets with finite drift velocity	- Simplified models that include the influence of small, sub-buoyant convective flows - Relies heavily on extensive data from ground-based facilities

5 Flight Experiment Requirements

5.1 Experiment Requirements

This section describes the experimental requirements and the rationale behind the requirements. A summary of all the requirements is provided in tabular form is first, followed by a more detailed explanation about the rationale behind the requirement.

Table 4: Hardware requirements tabulation.

Section	Description	Requirements
6.1.1	Test Fuels	- n-heptane (sooting) - methanol (non-sooting) - research grade, dry, degassed, purity greater than 99.5% - fuel temperature at the start of the test shall be in the range of 18 - 27 C
6.1.2	Droplet Deployment and Ignition	- 2 mm to 6 mm $\pm$ 0.25 mm and reproducible to within $\pm$ 5% - support fiber diameter $< 100\,\mu m$ and capable of anchoring droplet at a fixed location - hotwire ignition using minimum ignition energy following cessation of deployment-induced oscillations - igniter positioning shall be within 1-5 droplet radii away from surface, command controllable to within 0.5mm, and removable from the field of view - igniter power and duration of powered cycle shall be command controllable to provide ignition of droplet using the minimum ignition energy - a cylindrical volume of length $20D_0$ downstream, at least $8D_0$ upstream, and a diameter of $10D_0$ with the center located at the deployment site must be maintained free of any objects, where D_0 is the initial droplet diameter - capability of lighting within a flow field
6.1.3	Initial Pressure	- test pressures at 0.5, 1.0, 2.0 and 3.0 atm $\pm$ 0.05 atm - chamber pressure to be maintained within $\pm$ 10% of initial conditions throughout each test.
6.1.4	Initial Gas Composition	- mole fractions of O_2 from 0.10 to 0.40 - mole fractions of CO_2, He and SF_6 from 0 to 0.7 - mole fractions of N_2 from 0 to 0.79 - tolerance on initial charge is $\pm\,0.005$ for O_2, $\pm\,0.01$ for N_2, He, SF_6 and CO_2.
6.1.5	Misc. Ambient Requirements	- initial gas temperature at 18 - 27 C - humidity $<$ 10% for n-heptane and $<$ 2% for methanol - quiescent atmosphere prior to ignition - well-mixed gases prior to ignition.

6.1.6	Ambient Flow Conditions	- uniform upstream flow velocity within a cross-sectional flow diameter of 5.0 cm uniformity maintained within $\pm$ 1% of target velocity - target flow velocities between 0.1 cm/sec and 5 cm/sec, $\pm$1% - flow acceleration/deceleration controllable - direction of flow shall be perpendicular to the droplet support fiber
6.1.7	Operational Requirements	- allow at least 2 minutes after filling chamber to ensure gas temperature and pressure has stabilized - allow a 'droplet dwell time' of at least 10 sec to ensure all droplet motion imparted by droplet deployment and needle retraction has subsided - a 'near real time' downlink of the color camera video and the chamber gas pressure and temperature shall be provided - fuel vapor mole fraction of < 0.005 in the atmosphere - for chamber atmospheres that do not use CO_2 as a diluent the atmosphere shall consist of < 0.02 mole fraction (for each species) CO, CO_2 , and other products
6.1.8	Microgravity Requirements	-acceleration levels are required to be $2x10^{-6} - 2x10^{-4}$ on three axes depending on the size of the droplet - measurement accuracy shall be $1x10^{-6}$ - frequency range shall be $0.01 - 125\,Hz$ - sampling rate shall be $2 - 5$ times the frequency

5.1.1 Test Fuels

Two different liquid fuels will be used in FLEX experiments. The first is a sooting, alkane fuel (n-heptane) and the second is a non-sooting, alcohol fuel (methanol). Investigations of sooting and non-sooting fuels allow us to quantify the influences of sooting on extinction and burning dynamics, such as radiative output. Also, the chemical kinetics of alkanes and alcohols are fundamentally different due to the presence of oxygen molecules in the alcohol which will help explain effects of fuels on the absolute rankings of suppressant efficacy. In addition, since the Droplet Combustion Experiment 1 (DCE-1) used these fuels in a quiescent microgravity environment the data from DCE-1 provides a baseline for the FLEX experiments. These fuels have also been used in the FSDC and drop-tower experiments, and extensive chemical kinetic mechanisms exist.
Fuel Type: n-heptane (C_7H_{16}), an alkane fuel with a wide range of sooting behavior that vary depending on environmental conditions and methanol (CH_3OH), a non-sooting alcohol fuel
Fuel Purity: purity levels shall be the highest purity level that is commercially available (research grade at 99.5% by volume at present). Liquids shall be degassed and contain no H_2O
Quality Assurance: certification of test samples shall be provided prior to flight
Fuel Temperature: in the range of 18 - 27 C prior to the start of any test.

5.1.2 Droplet Deployment and Ignition

Droplet size during FLEX experiments is varied between 2 mm and 6 mm. A measured quantity of fuel is dispensed from a fuel reservoir and deposited onto the support fiber using a suitable deployment technique (e.g., opposed-needle technique used in DCE or single-needle technique implemented in the ground-based rigs). Hot-wire igniters are positioned at the proper location for ignition prior to deployment. Following deployment, after a preset dwell time designed to allow droplet surface oscillations to die out, the gas-phase fuel/oxidizer mixture is ignited using minimum ignition energy. Our previous experimental results show that deployment-induced droplet surface oscillations die out within a second. The ignition system should be capable of waiting for a predetermined duration for the oscillations to die out. After ignition, a cylindrical zone of exclusion axially aligned with the flow and radially centered at the droplet deployment site and extending 20 droplet diameters downstream and at least 8 droplet diameters upstream in length from the droplet center and having a diameter of 10 initial droplet diameters must be maintained free of any objects.
Droplet size: droplet diameter shall vary from $2\,mm$ to $6\,mm \pm 0.25\,mm$
Droplet reproducibility: droplet size shall be reproducible to within $\pm\,5\%$
Support fiber: support fiber diameter shall be less than $100\,\mu m$ and shall serve to anchor the droplet at a fixed location
Droplet Ignition: hotwire ignition (minimum ignition energy for both convective and quiescent ignition)
Igniter Positioning: igniter tip shall be positioned within $0.5 - 2.5\,D_0$ away from the anticipated droplet surface. The position of igniter tip shall be controllable by command to within $0.5\,mm$. The igniter tip shall be removed from viewing area upon ignition.
Igniter operation: the time of igniter power-up and duration of igniter operation shall be controllable by command and shall ignite droplet with the minimum ignition energy necessary to sustain combustion.
Zone of exclusion: a cylindrical zone of exclusion axially aligned with the flow and radially centered at the deployment site extending volume of length $20D_0$ downstream, at least $8D_0$ upstream, and a diameter of $10D_0$ radially centered at the deployment site must be maintained free of any objects (where D_0 is the droplet initial diameter).

5.1.3 Initial Pressure

The ambient pressure changes the sooting and radiation characteristics of the droplet.

Ambient pressure: initial ambient absolute pressure shall be set to $0.5 - 3.0\,atm \pm 0.05atm$.
Pressure transient:: chamber pressure shall be $\pm\,10\%$ of the initial ambient pressure throughout each test.

5.1.4 Initial Ambient

The ambient oxygen mole fraction influences the burning rate, extinction diameter, flame chemistry and flame characteristics (size, temperature). This parameter will vary from 0.4 down to the limit where no flame can be sustained at any droplet diameter (the LOI). The suppressants in the present study will have widely varying chemical and physical characteristics.

Oxygen Mole Fraction: oxygen mole fraction shall range from $0.1 - 0.4 \pm 0.005$.
Suppressant Type: CO_2, He and SF_6.
Suppressant Mole Fraction: suppressant mole fractions shall range from $0 - 0.7 \pm 0.01$.

5.1.5 Misc. Ambient Requirements

Balance: the diluent gas for all experiments will be nitrogen.
Ambient Quiescience: gases shall be well-mixed and quiescent (for the non-flow tests) prior to ignition.
Ambient temperature: - initial chamber gas temperature shall be $18 - 27\,C$.
Relative humidity: chamber relative humidity shall be less than 10% for the n-heptane test points and less than 2% for the methanol test points.

5.1.6 Ambient Flow Conditions

One objective of FLEX is to study slow convective flow effects on suppressant efficacy. Procedures must be implemented to assure the uniformity of the flow velocity accurately. To establish flow the droplet-support fiber mechanism is translated at a specified speed. This method provides precise control over the imposed flow and allows accurate control of the flow acceleration/deceleration, particularly at low speeds.

During combustion the droplet continually shrinks in size and the Reynolds number, based on instantaneous droplet diameter, continually decreases if the flow velocity is not increased with time. In order to maintain a desired Reynolds number during combustion and to study flow induced transient effects we need to control the flow velocity with prescribed acceleration/deceleration values under certain test runs. Therefore the flow control system should have the capability to decelerate or accelerate.

Flow velocities: target flow velocities from $0.1\,cm/sec$ to $5\,cm/sec \pm 1\%$.
Flow uniformity: uniform upstream flow velocity within a cross-sectional flow diameter of $5.0\,cm$ and uniformity maintained with $\pm 1\%$ of target velocity.
Flow direction: direction of flow shall be perpendicular to the droplet support fiber.
Flow acceleration/deceleration: flow acceleration/deceleration controllable

5.1.7 Operational Requirements

The chamber shall be filled with the appropriate atmosphere, which depending on the test point, will vary in pressure from 0.5 atm to 3.0 atm, will vary in O_2 concentration from 0.1 to 0.4 mole fraction, and will vary in suppressant concentration from 0 to 0.7 mole fraction. A settling time of approximately 2 minutes will elapse prior to initiating the test in order to ensure that the temperature and pressure of the chamber gases have stabilized. This settling time will be followed by the dispensing of a predetermined amount of fuel (based on the target droplet size) onto the support fiber. When sufficient fuel has been dispensed the dispensing needles will be retracted and a dwell period of at least 10 seconds will be allowed for the droplet internal fluid motion induced by deployment to subside. This will then be followed by initiating power to the igniter for a selectable amount of time ranging from 1 seconds to 5 seconds after which the igniter will be retracted from the field of view. If the flow field is to be generated by translating the droplet then droplet motion would commence at the same time that the igniter is retracted. A "near real-time" download of the

color camera video will be required in order to verify successful droplet deployment, ignition, and overall progress of the experiment. Pressure and temperature data of the chamber environment will also be required in "near real time".
Gas stabilization time: allow at least 2 minutes after filling chamber to ensure that the chamber gas temperature and pressure has stabilized.
Droplet dwell time: at least 10 seconds to ensure all droplet motion imparted by droplet deployment and needle retraction has subsided [6].
Real time downlink: a 'near real time' downlink of the color camera video and the chamber gas, pressure and temperature shall be provided.
Chamber Purity: fuel vapor mole fraction of < 0.005 in the atmosphere for tests without CO_2 ; < 0.02 mole fraction (each species) of CO, CO_2 and other products.

5.1.8 Microgravity Requirements

In order to compare the experimental data with theoretical results obtained under the conditions $Re \sim O(1)$ we need to minimize the effects of buoyancy on the flow field. The dimensionless parameter that compares the buoyancy effects to forced flow effects is the ratio of two dimensionless groups, the Gr/Re^2, where Gr is the Grashof number, and Re is the Reynolds number. The magnitude of this dimensionless group indicates the relative effect of buoyancy compared to forced convection and we need $Gr/Re^2 << 1$ in our experiments. This criterion can be translated into a requirement on the g-level as follows:

$$\frac{Gr}{Re^2} = \frac{g\,\beta\,\Delta T\,D}{U_\infty^2} << 1 \tag{5}$$

where g is the gravitational acceleration, β is the coefficient of thermal expansion, ΔT is the characteristic temperature difference, D is the characteristic length scale and U_∞ is the free-stream velocity. For the worst case scenario $\Delta T \sim 5$, $D \sim 1\,cm$ and $U_\infty \sim 1\,cm/s$ which yields a g/g_0 value of $1x10^{-5}$ as the required g-level (g_0 is the earth normal gravity).
Micro-gravity levels: accelerations are required to be less than $10^{-4}\,m/s^2$ in order to ensure buoyant forces are negligible.

5.2 Diagnostic Requirements

This section describes the diagnostic requirements and the rationale behind the requirements. A summary of all the requirements is provided in tabular form is first, followed by a more detailed explanation about the rationale behind the requirement.

[6] This time will be insufficient for large droplets, at least for damping of internal flows. Also internal flows within methanol droplets may never decay to low levels because of Marangoni effects, i.e., from water absorption).

Table 5: Diagnostic requirements tabulation.

Section	Description	Requirements
6.2.1	Droplet Imaging	- focal plane parallel to support fiber - FOV at least 3.0 cm centered on droplet (center of FOV) - resolution of 30 μm for smallest droplet size over entire FOV - frame rate at least 30 fps - depth of view at least 3.0 cm - some tests may be run in $2x2$ binned mode (at $60 - 100$ fps) with a ± 60 μm spatial resolution - ability to backlight the droplet
6.2.2	OH^* Flame Imaging	- focal plane parallel to support fiber - FOV at least 5.0 cm centered on droplet (center of FOV) - color detection for wavelengths of 310 nm $\pm 5nm$ - resolution of 100 μm - frame rate at least $30fps$ - depth of view at least 3.0 cm - adjustable gain
6.2.3	Color Flame Imaging (Experiment Monitoring Camera)	- full flame view with focal plane parallel to support fiber (preferred) - FOV at least 5.0 cm and positioned such that entire flame is imaged - resolution of 100 μm - frame rate at least 30 fps - depth of view at least 3.0 cm - near real- time downlink
6.2.4	Flame Radiation	- radiometer used to detect water vapor radiation shall be filtered to detect wavelengths in a band centered at 1.87 μm - radiometer used for broad-band radiation shall detect wavelengths within a band from $0.6 - 5.0$ μm - sample rate shall be at a frequency of 30 Hz - radiometers shall be shielded from all reflected and/or direct radiation from the igniter wire - radiometers shall be positioned at least 15 cm from the droplet to enable detection of all incident radiation from the flame. - accuracy 5% of full scale incident radiation - response time constant to be $<$ 40 ms - field of view shall be 65 mm diameter centered around the deployment site

6.2.5	Soot Volume Fraction	- camera shall provide full view of the droplet and flame with a preferred orientation such that the focal plane is parallel to the flow direction and coplanar with the droplet - backlit with wavelength of 660 nm and a FWHM of 5 nm - frame rate of 15 fps - FOV at least 5 cm about center of deployed droplet - resolution of 50 μm over the entire FOV
6.2.6	Soot Temperature	- focal plane shall be parallel to the flow direction and coplanar with and centered on the droplet - FOV at least 5 cm about the center of the deployed droplet - at least 7 fps for both wavelengths - resolution of 50 μm over the entire FOV - shall be adjustable prior to each test
6.2.7	Flow Velocity Measurement	- record translated motion (accelerated and steady) - sample rate shall be $\geq$ 30 Hz
6.2.8	Ambient Pressure and Temperature Measurement	- minimum sample rate shall be at 10 Hz - temperature accuracy shall be at least $\pm$ 0.5 C in the range of $18 - 27\,C$ - pressure accuracy shall be at least $\pm$ 0.01 atm in the range of $0.5 - 3\,atm$
6.2.9	Time Synchronization	- all measurements shall be referenced to GMT with a minimum accuracy of $\pm$ 0.03 sec

5.2.1 Droplet Imaging

A back-lit view of the droplet shall be provided that will allow accurate measurements of the droplet size as a function of time. This is necessary to obtain droplet burning rates and extinction droplet diameters. This view also yields quantitative regarding the soot shell and soot shell dynamics. The time resolution is necessary to accurately measure the burning rate constant and it's temporal variation as well as accurate measurements of the extinction droplet diameter.
Orientation: focal plane shall be aligned so that it is parallel with the fiber support axis and coplanar with the droplet
Field of view: minimum of 3.0 cm centered about the droplet
Resolution: 30 μm (i.e. $> 10\,lp/mm$) for the smallest droplet size over the entire FOV. Request higher framing rates for specified (TBD) tests. At 60-100 fps the spatial resolution shall be 60 μm.
Minimum frame rate: 30 fps over the duration of the test. Request the option to increase the frame rate to $>$ 60 fps although at reduced spatial resolution.

5.2.2 $OH*$ Flame Imaging

The flame structure and its dynamic response shall be obtained from flame imaging oriented perpendicular to the stream-wise flow direction. The flame image shall be derived from the ultraviolet OH-radical chemiluminescence emission intensity. This technique is well understood and has been implemented in a previous flight experiment (DCE-1).

Orientation: focal plane shall be parallel to the flow direction
Field of view: minimum of 5.0 cm
Depth of view: minimum 3.0 cm
Color: shall detect wavelengths of 310 $nm \pm 5nm$ using an intensified camera in order to detect $OH*$ radical emission.
Resolution: 100 μm (i.e. $> 5\, lp/mm$) over the entire FOV.
Minimum frame rate: 30 fps over the duration of the test.
Gain setting: shall be adjustable prior to each test.

5.2.3 Secondary Color Flame Imaging

A color CCD camera viewing the droplet at a specified angle will provide flame color information during combustion. Based on earlier flight experiments, it is also desired that this camera serve as the experiment's monitor camera to facilitate experiment operation/monitoring from the ground.
Orientation: camera shall provide full view of the droplet and flame with the focal plane parallel to the flow direction preferred; camera shall also provide viewing of the droplet dispensing and deployment sequence.
Field of view: minimum of 5.0 cm
Depth of view: minimum of 3.0 cm
Minimum frame rate: 30 fps over the duration of the test.
Downlink: image shall be down-linked in *near real-time* during each test.
Zoom: request the capability to 'zoom' (decreased FOV) this view for a more detailed view of the deployment, ignition and burning process for specified (TBD) tests.

5.2.4 Flame Radiation

Prior experimental results from DCE and FSDC have established that both luminous and non-luminous radiation play a significant role in flame extinction. These measurements will be used to obtain the total radiant energy loss as well as to establish the exact moment of flame extinction and to supplement other imaging data in determining transient flame behavior. Thermopile radiometers, positioned at distances far enough from the droplet to allow full view of the flame, will be used to measure *broad-band* radiation and water-vapor radiation from the flame zone.
Water vapor: radiometer used to detect water vapor radiation shall be filtered to detect wavelengths in a band centered at 1.87 μm (5.1 $-$ 7.5 μm)
Broad-band spectrum: radiometer used for broad-band radiation shall detect wavelengths within a band from 0.6 μm $-$ 5 μm.
Sample rate: data sampled from the radiometer shall be at a frequency of 30 Hz.
Positioning: radiometers shall be positioned at least 15 cm from the droplet to enable detection of all incident radiation from the flame.
Field of view: 65 mm centered on the deployment site
Response Time: time constant of less than 40 ms
Accuracy: 5% of full scale incident radiation

5.2.5 Soot Volume Fraction Measurement

It has long been established that the presence of soot will influence the droplet burning rate, the flame dynamics, and the flame extinction limits. Increased thermal radiation from the soot forming region, impacts on mass and thermal diffusion due to the physical presence of soot acting

as a barrier to the diffusive processes, and the changes in thermophysical properties in the fuel-rich region of the diffusion flame due to varying levels of soot concentration all contribute to changes in the dynamics of the droplet burning and extinction behavior. In order to assess these influences with the n-heptane droplet tests it is *desired* to quantify soot concentration levels by obtaining soot volume fraction measurements within the diffusion flame.

An established technique for making this measurement has been to use a multi-chord, line-of-sight light extinction measurement coupled with an inversion technique to obtain soot volume fraction distributions. This requires a backlight using a collimated laser light source of known intensity and by discriminating that intensity from the flame emission and stray light by using combinations of interference and neutral density filters. It is anticipated that this measurement, if available, will use the HiBMS camera with the appropriate spectral filtering, typically $660\,nm$ with a FWHM (full width half maximum) of $5\,nm$, and with an appropriate intensity resolution, which is typically require a minimum of 8 bits of dynamic range.
Orientation: camera shall provide full view of the droplet and flame with a preferred orientation such that the focal plane is parallel to the flow direction and coplanar with the droplet.
Backlit illumination: collimated light source with a wavelength of $660\,nm$ and a FWHM of $5\,nm$
Frame rate: frame rate shall be at least $7\,fps$
Field of view: a FOV shall be at least $5.0\,cm\,x\,5.0\,cm$
Resolution: $50\,\mu m$ (i.e. $>\,10\,lp/mm$) over the entire FOV.

5.2.6 Soot/Fiber Temperature

In addition to knowing the soot volume fraction, Eq. 3 shows that it is equally, if not more, important to know the soot temperature. Therefore, it is *desired* to quantify the soot temperature (and SiC fiber temperature) to obtain quantitative information regarding the broadband radiation due to soot. An established technique for making soot temperature measurements and one that has been successfully implemented in ground-based facilities is multi-wavelength pyrometry. This measurement could use the CIR HiBMS camera with the Liquid Crystal Tunable Filter (LCTF). Limitations on the CIR/MDCA hardware likely preclude two cameras each imaging a different wavelength. The framing rate of the camera, combined with rapid temporal response of the LCTF make it feasible to make measurements on successive frames at the two different wavelengths. Assuming minimal changes in soot volume fraction and temperature during the inter-frame time, it is then possible to measure the soot temperature. Also, with no additional hardware, this same system could measure the temperature of the SiC support fiber (during non-sooting tests) to get a measure of the gas-phase flame temperature.
Orientation: camera shall provide full view of the droplet and the flame with a preferred orientation such that the focal plane of the camera is parallel to the support fiber.
Frame Rate: frame rate shall be at least $7\,fps$
Field of View: the FOV shall be at least $5.0\,cm\,x\,5.0\,cm$ about the center of the deployed droplet
Resolution: $50\,\mu m$ (i.e. $>\,10\,lp/mm$) over the entire FOV.

5.2.7 Flow Velocity Measurement

It is important that the instantaneous free-stream velocity is known accurately during the entire combustion process. If measurements are not feasible an indirect feed-back related to velocity through calibration should be provided.
Sample Rate: at least $30\,Hz$

5.2.8 Ambient Temperature and Pressure Measurement

During each test the chamber gas temperature and pressure measurements shall be required. The following are the specifications for this data.
Sample rate: minimum sample rate shall be at 10 Hz
Temperature: accuracy shall be at least $\pm\, 0.5C$.
Pressure: accuracy shall be at least $\pm\, 0.01\ atm$.

5.2.9 Synchronization

Experiment objectives require all data to be time-synchronized to a reference time. This will allow accurate interpretation of the data and evaluate droplet regression rate, flame structure, and flame extinction as a function of time.
Time synchronization: all measurements shall be referenced to GMT with a minimum accuracy of $\pm\, 0.03\ sec$.

5.3 Flight Experiment Test Procedures

The FLEX experiments involve igniting and observing the burning behavior of relatively large droplets. One of the primary objectives of the experiments is to determine the LOI as a function of ambient pressure and determine how the presence of a suppressant influences the LOI . The determination of the LOI involves conducting a series of tests and constructing a diagram similar to that in Fig. 2. The basic outline of the procedure to construct this diagram is as follows:

1. Select the test pressure ($0.5\ -\ 1.5\ atm$) for the LOI tests.
2. Select a smaller droplet size ($\approx\ 3\ mm$)
3. Select an ambient oxygen mole fraction that, based on ground-based testing, will support droplets burning to completion (as opposed to extinguishing at a finite droplet size).
4. Perform a droplet combustion test.
5. Increase the droplet size or repeat the test (if finite extinction diameter at flame extinction observed).
6. Continue steps 4 and 5 until flame exists for only a short time after ignition (radiative extinction).
7. Continue steps 4 thru 6 at a decreased ambient oxygen mole fraction.
8. Continue step 7 to an ambient oxygen mole fraction where the droplet does not ignite.

There will likely be ambient conditions where the extinction droplet sizes at all ambient oxygen mole fractions are too small to either be observed or measured with the available diagnostics. In this case, the determination of the LOI is similar, but more iterative. Instead of observing flame extinction, however, the procedure will involve an iterative sequence of tests (burn to completion followed by a no ignition test) with progressively smaller increments in ambient oxygen mole fraction to determine the LOI .

For the slow flow tests (in the flight experiment), the current configuration of the flight hardware does not allow for adequate diagnostics over the entire test for a droplet in a uniform, steady

convective flow[7]. In these tests, the procedure will be to duplicate tests above which yield finite-sized extinction droplet diameters. Near the end of the tests, prior to flame extinction, the droplet will by subjected to a small, sub-buoyant, convective flow (imparted by translating the droplet at a slow, uniform speed). The goal of the experiment is then to see how the presence of this flow influences the extinction process. We also note that a large number of the tests will involve free droplets (as opposed to fiber-supported droplets). A number of these tests will have droplets with a slow drift velocity. We can also use the data gathered from these tests to examine the influences of a small, sub-buoyant flow on both the burning and extinction process.

The procedure to examine the suppressant efficacy will be essentially the to that used to determine the LOI . The major difference will be that in addition to the diluent (N_2), the ambient will contain a suppressant. The test procedure will be identical to that above; the steps described above will be performed at a fixed suppressant level. Subsequent series of tests will then be at different suppressant concentrations and types of suppressants.

5.4 FLEX Test Matrix

The proposed test matrix is fashioned so as to meet the stated science objectives and at the same time meet the constraints imposed by the hardware as well as the safety requirements of space experiments. The previous section described the test procedures. The exact test matrix will change during the conduct of the FLEX experiment. The initial conditions for the first series of FLEX tests will be determined by extensive ground testing in the drop towers at the NASA Glenn Research Center. It is important, however, for the engineering team to have a test matrix on paper so that it can determine consumable resource requirements and prepare for the necessary safety reviews. The following test matrices, then are designed to allow the engineering team to adequately plan for the experiment and do not represent the final test matrix. These test matrices provide for an envelope in which all of the actual tests will be conducted.

The test matrix is broken up into a series of sub-matrices each of which is designed to highlight an objective of the experiment. The first series of tests, described in Tables 6 and 7, will determine the LOI as a function of pressure for heptane and methanol in quiescent and flowing environments, respectively. The second series of tests, described in Tables 8, 9 and 10, examines the efficacy of CO_2 , He and SF_6 . The tests use the two test fuels, are over a range of pressures, oxygen mole fractions and suppressant mole fractions. The tests described in Table 11 examine how a slow, sub-buoyant flow influences the efficacy of a single suppressant, CO_2 . Finally, the tests in Table 12 examine the influence of a stronger radiative environment (achieved by increasing the pressure) on the efficacy of a single suppressant.

[7]This will, however, be extensively studied in the complimentary ground-based program

Table 6: Quiescent environment LOI test matrix.

Fuel: C_7H_{16} , Diluent: N_2 , No fiber support, Flow: $0.0\,cm/s$, $D_0 = 3,\,5\,mm$, $X_{N2} = 1.0 - X_{O2}$.		
Test No.	$P\,(atm)$	X_{O2}
1	0.50	0.20
2	0.50	0.30
3	0.50	0.35
4	0.75	0.13
5	0.75	0.20
6	0.75	0.28
7	0.75	0.40
8	1.00	0.10
9	1.00	0.15
10	1.00	0.21
11	1.00	0.30
12	1.50	0.10
13	1.50	0.15
14	1.50	0.21
Fuel: CH_3OH		
15	0.50	0.20
16	0.50	0.30
17	0.50	0.35
18	0.75	0.13
19	0.75	0.20
20	0.75	0.28
21	0.75	0.40
22	1.00	0.10
23	1.00	0.15
24	1.00	0.21
25	1.00	0.30
26	1.50	0.10
27	1.50	0.15
28	1.50	0.21

Table 7: Slow flow LOI test matrix

Fuel: C_7H_{16} , Diluent: N_2 , SiC fiber support, Flow: $1.5\,cm/s$, $D_0 = 3,\ 5\,mm$, $X_{N2} = 1.0 - X_{O2}$.		
Test No.	$P\,(atm)$	X_{O2}
29	0.50	0.20
30	0.50	0.30
31	0.50	0.35
32	0.75	0.13
33	0.75	0.20
34	0.75	0.28
35	0.75	0.40
36	1.00	0.10
37	1.00	0.15
38	1.00	0.21
39	1.00	0.30
Fuel: CH_3OH		
40	0.50	0.20
41	0.50	0.30
42	0.50	0.35
43	0.75	0.13
44	0.75	0.20
45	0.75	0.28
46	0.75	0.40
47	1.00	0.10
48	1.00	0.15
49	1.00	0.21
50	1.00	0.30

Table 8: CO_2 suppressant efficacy test matrix.

Fuel: C_7H_{16} , Diluent: N_2 , Suppressant: CO_2 , No fiber support, Flow: $0.0\,cm/s$, $D_0 = 3,\ 5\,mm$, $X_{N2} = 1.0 - X_{O2} - X_{CO2}$.			
Test No.	$P\,(atm)$	X_{O2}	X_{CO2}
51	0.70	0.25	0.15
52	0.70	0.25	0.25
53	0.70	0.25	0.50
54	0.70	0.25	0.70
55	0.70	0.30	0.15
56	0.70	0.30	0.25
57	0.70	0.30	0.50
58	0.70	0.30	0.70
59	0.85	0.25	0.15
60	0.85	0.25	0.25
61	0.85	0.25	0.50
62	0.85	0.25	0.70
63	0.85	0.30	0.15
64	0.85	0.30	0.25
65	0.85	0.30	0.50
66	0.85	0.30	0.70
67	1.00	0.10	0.15
68	1.00	0.10	0.25
69	1.00	0.10	0.50
70	1.00	0.10	0.70
71	1.00	0.15	0.15
72	1.00	0.15	0.25
73	1.00	0.15	0.50
74	1.00	0.15	0.70
75	1.00	0.21	0.15
76	1.00	0.21	0.25
77	1.00	0.21	0.50
78	1.00	0.21	0.70
Fuel: CH_3OH .			
79	0.70	0.25	0.15
80	0.70	0.25	0.25
81	0.70	0.25	0.50
82	0.70	0.25	0.70
83	0.70	0.30	0.15
84	0.70	0.30	0.25
85	0.70	0.30	0.50
86	0.70	0.30	0.70
87	0.85	0.25	0.15
88	0.85	0.25	0.25
89	0.85	0.25	0.50
90	0.85	0.25	0.70

91	0.85	0.30	0.15
92	0.85	0.30	0.25
93	0.85	0.30	0.50
94	0.85	0.30	0.70
95	1.00	0.10	0.15
96	1.00	0.10	0.25
97	1.00	0.10	0.50
98	1.00	0.10	0.70
99	1.00	0.15	0.15
100	1.00	0.15	0.25
101	1.00	0.15	0.50
102	1.00	0.15	0.70
103	1.00	0.21	0.15
104	1.00	0.21	0.25
105	1.00	0.21	0.50
106	1.00	0.21	0.70

Table 9: He suppressant efficacy test matrix.

Fuel: C_7H_{16} , Diluent: N_2 , Suppressant: He , No fiber support, Flow: $0.0\,cm/s$, $D_0 = 3,\ 5\,mm$, $X_{N2} = 1.0 - X_{O2} - X_{He}$.			
Test No.	$P\,(atm)$	X_{O2}	X_{He}
107	0.70	0.25	0.15
108	0.70	0.25	0.25
109	0.70	0.25	0.50
110	0.70	0.25	0.70
111	0.70	0.30	0.15
112	0.70	0.30	0.25
113	0.70	0.30	0.50
114	0.70	0.30	0.70
115	0.85	0.25	0.15
116	0.85	0.25	0.25
117	0.85	0.25	0.50
118	0.85	0.25	0.70
119	0.85	0.30	0.15
120	0.85	0.30	0.25
121	0.85	0.30	0.50
122	0.85	0.30	0.70
123	1.00	0.10	0.15
124	1.00	0.10	0.25
125	1.00	0.10	0.50
126	1.00	0.10	0.70
127	1.00	0.15	0.15
128	1.00	0.15	0.25
129	1.00	0.15	0.50
130	1.00	0.15	0.70
131	1.00	0.21	0.15
132	1.00	0.21	0.25
133	1.00	0.21	0.50
134	1.00	0.21	0.70
Fuel: CH_3OH			
135	0.70	0.25	0.15
136	0.70	0.25	0.25
137	0.70	0.25	0.50
138	0.70	0.25	0.70
139	0.70	0.30	0.15
140	0.70	0.30	0.25
141	0.70	0.30	0.50
142	0.70	0.30	0.70
143	0.85	0.25	0.15
144	0.85	0.25	0.25
145	0.85	0.25	0.50
146	0.85	0.25	0.70

147	0.85	0.30	0.15
148	0.85	0.30	0.25
149	0.85	0.30	0.50
150	0.85	0.30	0.70
151	1.00	0.10	0.15
152	1.00	0.10	0.25
153	1.00	0.10	0.50
154	1.00	0.10	0.70
155	1.00	0.15	0.15
156	1.00	0.15	0.25
157	1.00	0.15	0.50
158	1.00	0.15	0.70
159	1.00	0.21	0.15
160	1.00	0.21	0.25
161	1.00	0.21	0.50
162	1.00	0.21	0.70

Table 10: SF_6 suppressant efficacy test matrix.

Fuel: C_7H_{16} , Diluent: N_2 , Suppressant: SF_6 , No fiber support, Flow: $0.0\,cm/s$, $D_0 = 3,\ 5\,mm$, $X_{N2} = 1.0 - X_{O2} - X_{SF6}$.			
Test No.	$P\,(atm)$	X_{O2}	X_{SF6}
163	0.70	0.25	0.15
164	0.70	0.25	0.25
165	0.70	0.25	0.50
166	0.70	0.25	0.70
167	0.70	0.30	0.15
168	0.70	0.30	0.25
169	0.70	0.30	0.50
170	0.70	0.30	0.70
171	0.85	0.25	0.15
172	0.85	0.25	0.25
173	0.85	0.25	0.50
174	0.85	0.25	0.70
175	0.85	0.30	0.15
176	0.85	0.30	0.25
177	0.85	0.30	0.50
178	0.85	0.30	0.70
179	1.00	0.10	0.15
180	1.00	0.10	0.25
181	1.00	0.10	0.50
182	1.00	0.10	0.70
183	1.00	0.15	0.15
184	1.00	0.15	0.25
185	1.00	0.15	0.50
186	1.00	0.15	0.70
187	1.00	0.21	0.15
188	1.00	0.21	0.25
189	1.00	0.21	0.50
190	1.00	0.21	0.70
Fuel: CH_3OH			
191	0.70	0.25	0.15
192	0.70	0.25	0.25
193	0.70	0.25	0.50
194	0.70	0.25	0.70
195	0.70	0.30	0.15
196	0.70	0.30	0.25
197	0.70	0.30	0.50
198	0.70	0.30	0.70
199	0.85	0.25	0.15
200	0.85	0.25	0.25
201	0.85	0.25	0.50
202	0.85	0.25	0.70

203	0.85	0.30	0.15
204	0.85	0.30	0.25
205	0.85	0.30	0.50
206	0.85	0.30	0.70
207	1.00	0.10	0.15
208	1.00	0.10	0.25
209	1.00	0.10	0.50
210	1.00	0.10	0.70
211	1.00	0.15	0.15
212	1.00	0.15	0.25
213	1.00	0.15	0.50
214	1.00	0.15	0.70
215	1.00	0.21	0.15
216	1.00	0.21	0.25
217	1.00	0.21	0.50
218	1.00	0.21	0.70

Table 11: Suppressant efficacy in a slow flow test matrix.

Fuel: C_7H_{16} , Diluent: N_2 , Suppressant: CO_2 , No fiber, Flow: $1.5\,cm/s$, $D_0 = 3,\ 5\,mm$, $X_{N2} = 1.0 - X_{O2} - X_{CO2}$.			
Test No.	$P\,(atm)$	X_{O2}	X_{CO2}
219	0.70	0.10	0.15
220	0.70	0.10	0.25
221	0.70	0.10	0.50
222	0.70	0.10	0.70
223	0.70	0.21	0.15
224	0.70	0.21	0.25
225	0.70	0.21	0.50
226	0.70	0.21	0.70
227	1.00	0.10	0.15
228	1.00	0.10	0.25
229	1.00	0.10	0.50
230	1.00	0.10	0.70
231	1.00	0.15	0.15
232	1.00	0.15	0.25
233	1.00	0.15	0.50
234	1.00	0.15	0.70
235	1.00	0.21	0.15
236	1.00	0.21	0.25
237	1.00	0.21	0.50
238	1.00	0.21	0.70
Fuel: CH_3OH			
239	0.70	0.10	0.15
240	0.70	0.10	0.25
241	0.70	0.10	0.50
242	0.70	0.10	0.70
243	0.70	0.21	0.15
244	0.70	0.21	0.25
245	0.70	0.21	0.50
246	0.70	0.21	0.70
247	1.00	0.10	0.15
248	1.00	0.10	0.25
249	1.00	0.10	0.50
250	1.00	0.10	0.70
251	1.00	0.15	0.15
252	1.00	0.15	0.25
253	1.00	0.15	0.50
254	1.00	0.15	0.70
255	1.00	0.21	0.15
256	1.00	0.21	0.25
257	1.00	0.21	0.50
258	1.00	0.21	0.70

Table 12: Suppressant in a radiative environment test matrix.

Fuel: C_7H_{16} , Diluent: N_2 , Suppressant: CO_2 , No fiber support, Flow: $0.0\,cm/s$, $D_0 = 3,\ 5\,mm$, $X_{N2} = 1.0 - X_{O2} - X_{CO2}$.			
Test No.	$P\,(atm)$	X_{O2}	X_{CO2}
259	2.00	0.10	0.15
260	2.00	0.10	0.25
261	2.00	0.10	0.50
262	2.00	0.10	0.70
263	2.00	0.21	0.15
264	2.00	0.21	0.25
265	2.00	0.21	0.50
266	2.00	0.21	0.70
267	3.00	0.10	0.15
268	3.00	0.10	0.25
269	3.00	0.10	0.50
270	3.00	0.10	0.70
271	3.00	0.21	0.15
272	3.00	0.21	0.25
273	3.00	0.21	0.50
274	3.00	0.21	0.70
Fuel: CH_3OH			
275	2.00	0.10	0.15
276	2.00	0.10	0.25
277	2.00	0.10	0.50
278	2.00	0.10	0.70
279	2.00	0.21	0.15
280	2.00	0.21	0.25
281	2.00	0.21	0.50
282	2.00	0.21	0.70
283	3.00	0.10	0.15
284	3.00	0.10	0.25
285	3.00	0.10	0.50
286	3.00	0.10	0.70
287	3.00	0.21	0.15
288	3.00	0.21	0.25
289	3.00	0.21	0.50
290	3.00	0.21	0.70

6 Post-Flight Data Analysis

6.1 Flight Data Analysis Plan

The data reduction, analysis, dissemination of results, and eventual archiving of the experimental data will occur under the direction of the Research Team Leader. There will be extensive reliance on all of the team members, along with their support staff, in the analysis of data and with the formulation and publication of any conclusions that are derived from the experiments. It is anticipated that a number of graduate students will be intimately involved with the data reduction and analysis, development of theoretical models, and numerical simulations.

The primary scientific data obtained during these experiments will be the time histories of droplet diameter, flame shape, and radiant energy output by the flame, and possibly soot volume fraction measurements. These time evolutions are obtained for a given environmental condition (pressure and oxygen and suppressant concentration) at different initial droplet diameters and translation velocities. This data will provide the critical information necessary to validate and improve theoretical and numerical models of droplet combustion that can in turn lead to simplified sub-models of phenomena relevant to 'real fire' simulations.

All of the data from the flight experiment will be stored and archived electronically in an open-source format such as the Hierarchical Data Format. This includes scientific image and radiometric data as well as housekeeping data such as chamber temperature, pressure, etc. The GRC investigators will be responsible for archiving the raw and analyzed experimental data. It is expected that the information will be publicly available within 2 years from the completion of the flight experiment.

6.1.1 Temporal Droplet History

The measurement of the droplet history comes from the recorded backlit image data by measuring the size of the droplet as a function of time before and after ignition. The droplet burning rate and extinction droplet diameter are derived from this data. If soot volume fraction measurements are not available, then this image also contains qualitative information about the degree of sooting and soot shell location. This determination of accurate size measurements requires an accurate scale factor, and good edge discrimination. Choi et al. (1989); Struk et al. (1998) review the analysis procedures in detail. The software procedures exist and are routinely used by all of the investigators to analyze droplet combustion data.

The archived data will include the raw images from the CIR HiBMS camera along with the camera settings, illumination package details and scale factors. Additional archived data will include, at a minimum, analyzed data of the equivalent droplet size as a function of time, the initial and extinction droplet sizes, droplet shape (for fiber supported droplets).

6.1.2 Flame Shape and Structure

Two cameras provide flame images as a function of time, the $OH*$ image and the view from a color CCD camera. There is a large amount of data derived from these views including, but not limited to flame size and shape as a function of time, radial $OH*$ profiles (Marchese et al., 1996), flame luminosity and color (qualitative measures of soot formation/destruction) as functions of time, and the time of flame extinction. Accurate measurements require that the droplet be in focus and that appropriate scale factors are available. The procedures for flame size analysis are similar to those used in previous droplet tower and spaceflight experiments(Marchese et al., 1996; Ackerman et al.,

2003). In order to accurately measure extinction droplet diameter and flame standoff ratio, this data must be accurately time stamped and time correlated to the backlit droplet view.

The archived data will include the raw images from both the $OH*$ and color CCD cameras along with all of the camera settings and calibrations, and scale factors. Additional analyzed data will include, at a minimum, flame size, shape, relative luminosity, Abel-transformed $OH*$ profiles and time of flame extinction.

6.1.3 Soot Volume Fraction

The CIR laser illumination package along with the CIR HiBMS camera and the Liquid Crystal Tunable Filter (LCTF) can be used to measure the location and concentrations of soot using a light extinction technique (Choi and Lee, 1996). While this measurement is not required, it is strongly recommended because of the importance of soot formation, radiation and destruction to droplet burning. Accurate measurements of soot volume fraction require a well-characterized and calibrated light source and detector (camera). This data must be accurately time stamped and correlated with the flame and radiometric data to accurately quantify the influence of soot on the burning and extinction process.

If this measurement is available, then the archived data will include the raw images from the HiBMS camera along with all of the camera settings, calibrations, scale factors and calibration and characterization data for the light source. Additional analyzed data will include, at a minimum, radial profiles of soot volume fraction as a function of time and peak soot volume fractions.

6.1.4 Flame Radiation

Data obtained from both the wide and narrow band radiometers will be used to measure the non-luminous flame radiation. Accurate measurements require calibrated radiometers with well-defined spectral characteristics. In order to be useful in extracting extinction information and obtain ratios of radiative heat loss to combustion heat release, the data must be accurately time stamped and correlated with the flame, droplet and soot image data.

The archived data will include the raw radiometer data, the calibration factors and view factor information (geometry of the radiometer relative to the droplet). Analyzed data will include, at a minimum,

6.2 Science Success Criteria

In order to gauge the level of experimental success, criteria for two levels of success, minimal and complete success, have been defined in this section. Minimal Success requires that the measurements listed below are successfully obtained for a sufficiently representative set of test points to the extent that some meaningful conclusions related to the Science Objectives, as defined in Section 5.1, can be made. Complete Success requires that all the measurements listed below, for a sufficiently representative set of test points, are successfully obtained. Consequently, it is not necessary to actually have successfully completed each test point defined in the Test Matrix (Section 6.6) for complete science success as long as all the Science Objectives can be completely addressed. Additional test points, beyond those that are required for *complete* success, are requested in order to provide additional clarity and refinement to any conclusions that will be reached and to provide increased resolution to the resulting data base from which model validation will proceed.

6.2.1 Minimal Success

In order for the flight experiment to be considered minimally successful, the FLEX team must acquire a minimal set of data to allow validation of the theoretical/numerical models over a minimal range of ambient conditions. There must be sufficient data to allow quantitative measures that each objective in Section 5.1 is minimally met.

- Obtain droplet diameter and either $OH*$ or color video flame measurements as function of time for both methanol and heptane at two pressures over a range of droplet sizes and oxygen concentrations to adequately define the LOI .

- Perform the same measurements above with a slow flow imparted to the droplet near extinction (achieved by translating the droplet) for at least 5 droplets.

- Obtain droplet history and either $OH*$ or color video flame measurements as a function of time for both methanol and heptane for one pressure, two different oxygen concentrations and four CO_2 suppressant mole fractions.

- Obtain the same data for CO_2 cited above for one additional suppressant (He or SF_6).

- Perform the same measurements above with a slow flow imparted to the droplet near extinction for at least 10 droplets.

- Acquire droplet diameter, either $OH*$ or color video flame measurements and radiometric data (from both radiometers) at two pressures, two oxygen mole fractions and four suppressant mole fractions with CO_2 as the suppressant for both test fuels.

- Acquire droplet diameter, soot volume fraction and temperature and radiometric data for both fuels at high pressure and high ambient oxygen mole fraction ($P = 3.0\,atm$, $X_{O2} = 0.21$ in Table 12) and two CO_2 concentrations.

The data must be of sufficient quality to extract as a minimum reasonably accurate droplet size and flame size data. The ambient conditions inside the chamber must also be sufficiently well defined to allow meaningful comparisons between tests and with the theoretical/numerical models.

6.2.2 Complete Success

In order for the flight experiment to be considered completely successful all of the available diagnostics must be performed for all of the droplet combustion tests. This includes the following additions to the criteria for minimal success above.

- Both flame views and radiometric data for a complete range of oxygen mole fractions and at least four ambient pressures.

- Both flame views and radiometric data for at least 10 tests.

- Both flame views and radiometric data for three pressures and four ambient oxygen mole fractions.

- The same data above for at least three suppressants.

- The same data above with a slow flow imparted to the droplet near extinction for at least 10 droplets. A fraction of these tests (1/4) should include soot volume fraction and temperature measurements.

- Both flame views, radiometric data and soot volume fraction and temperature measurements for at least three pressures and four ambient oxygen mole fractions.
- Both flame views, radiometric data and soot volume fraction and temperature measurements for two pressures, two ambient oxygen mole fractions and four suppressant concentrations.

7 Ground-Based Research Program

There are four primary objectives to the ground-based FLEX research program. The first goal is to use the drop towers and reduced gravity aircraft (when appropriate) to develop the procedures and hardware settings necessary to ensure satisfactory operation on orbit. This portion of the ground-based program is typically handled by the engineering team and is not covered by this document. The second component is to take data that will be used to determine the final FLEX test matrix. The third component of the ground-based research program is to perform experiments to compliment the flight-based data. The final component of the ground-based research program is the development of the theoretical and numerical tools necessary to extend and generalize the results of droplet combustion experiments to suppression of more 'realistic' fires. Finally, we should note that these objectives are not mutually exclusive and results from some experiments can have multiple purposes (e.g. tests can be used to refine the test matrix and validate the numerical model).

7.1 Test Matrix Determination

Section 6.5 describes the test procedure for the flight experiments. One of the primary goals of these experiments is to use the experimental data of flame extinction to validate and refine chemical kinetic models. It is impossible to know *a priori* the ambient conditions that will yield measurable extinction droplet diameters (thus the need for the experiments). We do, however, need reliable estimates to optimize the use of the limited resources available on orbit. Therefore, we will implement a comprehensive test program to refine the initial test matrix prior to flight. This will consist of testing in the NASA GRC 2.2 and 5.2 second drop towers.

The tests will be conducted under the supervision of the GRC FLEX investigators and in consultation with all members of the FLEX engineering and external science team. The experiments will utilize a number of drop rigs available at GRC. These include the convective flow drop rig, the universal drop rig and possibly the droplet array test rig. All of these rigs exist and are operational or can be made operational with minimal work.

The ambient environments will be limited to those available on orbit for these tests. The diagnostics will include backlit images of the flame and an orthogonal view of the flame with the potential for radiometric measurements. The ignition energy and igniter configuration will be similar to that in the flight experiments. The goal of these experiments is to, in conjunction with the theoretical/numerical modeling efforts, to identify those conditions that are close to the flammability limits and likely to yield finite, measurable extinction droplet diameters.

7.2 Complimentary Experiments

The resources available to the flight experiment, while considerable for the flight experiments, are nevertheless limited in the context of covering all of the potential suppressants, fuels and ambient atmospheres. Therefore the FLEX team will conduct wide ranging experiments in the ground-based facilities at NASA GRC to provide additional scientific data for comparison to the flight-based data. This includes tests at smaller droplet sizes and higher oxygen concentrations (that can burn to completion in time available in the drop towers). This also includes tests using suppressants not allowed in the space flight experiments (for safety reasons). These suppressants include a wide range of chemically active suppressants that may produce chemical by-products at levels not allowed on the ISS.

These tests will be conducted by all of the FLEX team members under the direction of the FLEX Research Team Lead (F.A. Williams, University of California, San Diego). It is expected,

however, that all of the FLEX scientific team members will have a great deal of autonomy in deciding and pursuing areas of research that they feel are complimentary to the FLEX program. There are a number of test rigs available to support this testing. This includes, but is not limited to, drop rigs at Drexel University (capable of soot volume fraction measurements), the University of California, Davis (capable of tests at high pressures), Princeton University, and several at the NASA GRC. Most of these test rigs are for droplets burning in quiescent ambient (free-floating and fiber-supported). Two additional rigs at NASA GRC have the capability to study slow convective droplet combustion in the 2.2 and 5.2 second drop towers. These experiments can study flow velocities in the range of 0 to 3 cm/s and droplet diameters in the range 1 to 3 mm (Nayagam et al., 2003; Hicks et al., 2003) in a variety of ambient conditions.

7.3 Theoretical/Numerical Model Development

The experimental results (flight and ground-based) from the FLEX program will provide the data necessary to validate the theoretical and numerical models that will also be developed as a part of the FLEX program. These models include the continued development of a comprehensive numerical model of droplet combustion with detailed chemistry, transport and radiation. It also includes the development of validated, simplified models of chemistry, transport and radiation and theoretical models of droplet combustion to predict flame extinction, convective flow effects, etc.

F.L. Dryer of Princeton University will supervise the continued development of the comprehensive detailed numerical model. This will include incorporating the chemical kinetic mechanisms for the various suppressants and validating the performance against the ground-based and flight experimental data. The principal efforts under this program will be:

1. Refine the detailed chemical kinetic mechanisms for n-heptane, methanol, and ethanol, including soot precursor and sooting components. The work will also include computations using mechanisms for larger hydrocarbons such as n-decane and n-hexadecane to investigate the effects of higher hydrocarbon characteristics on fire safety parameters theoretically.

2. Incorporate sub-mechanisms for production of soot precursors and model components for nucleation, growth, coagulation, thermophoretic transport, and oxidation of soot particulates.

3. Complete efforts to produce more robust, but simplified modeling approaches for internal liquid phase transport from induced liquid phase motions.

4. Incorporate two dimensional, axi-symmetric effects of low gas/drop convection.

5. Develop and test low dimensional sub-mechanisms that continue to reproduce both experimental observations and predictions yielded from the detailed models. Studies have already been initiated studies to evaluate the effects of inert substitution and inert dilution on combustion properties of isolated droplets without convection (Kroenlein et al., 2004). These calculations are continuing to assist in refining test matrix conditions for experiments with CO2, He, and SF6 as the considered inert. Some experimental work has already occurred at NASA Glenn Research Center in the 2.2 and 5 s drop towers on dilution effects, and will be compared with calculations in the near future.

B.D. Shaw at the University of California, Davis will utilize and further develop the modeling effort to examine fiber effects on droplet combustion. The model currently simulates the vaporization of a fiber-supported droplet. The code is based on overset grid technology and presently uses three grids to model a droplet on a fiber. There is an overall major grid, which is cylindrical

in shape. This grid extends to the boundaries of the computational/physical space. A minor grid is fit to the droplet and the third grid is fit to the fiber. This model includes detailed transport, heat transport along the fiber and solutal and thermal Marangoni flows. Prof. Shaw will direct the effort to modify this code to simulate combustion of a fiber-supported droplet.

8 Management Plan

The FLEX Research Team Lead, F.A. Williams, maintains overall responsibility for the FLEX research program. All major decisions regarding the FLEX flight experiment and ground-based research program rest with the Research Team Lead. It is fully expected, however, that all of the external and internal GRC investigators will have a great deal of autonomy in the *day to day* operations of their own research. This includes the preparation of test plans and conducting experiments and analyzing and reporting the resulting data. All of the participating will meet and talk periodically to discuss flight hardware developments, research results and discuss relevant issues. All team members will report the results of their results to NASA in the form of periodic progress reports and more importantly to the peer community in technical meetings and journal publications. The Research Team Lead is responsible for the reporting the results of the research (specifically the items specified in Section 5.4) at the conclusion of the FLEX project.

The primary *day to day* responsibility for the flight hardware rests with the GRC investigators, V. Nayagam and M. Hicks. The are responsible for the daily interactions with the hardware development team, reviewing flight hardware performance documentation and test results and supervising the ground-based experiments that impact the development of the detailed test matrix and flight hardware. The internal investigators will keep the entire FLEX team updated on the results of testing and status of the flight hardware. Any critical decisions regarding the flight experiments are the responsibility of the Research Team Lead in consultation with all of the FLEX team members.

The analysis of the ground-based data will be the responsibility of the researcher who acquires the data. The analysis of the flight data will be jointly performed by the entire FLEX team under the direction of the FLEX Research Team Lead. The archiving of the flight experimental data in an open-source, publicly available format will be the responsibility of the GRC team members under the supervision of the FLEX Research Team Lead.

The development of the detailed numerical model will be the responsibility of F.L. Dryer. This includes code development, incorporation of *state of the art* sub-models of radiation, chemical kinetics, transport, etc. and validation of the model against both the space-flight and ground-based data.

9 Justification for Reduced Gravity

The objective of this experiment is to use the droplet as a model geometry for investigating suppressant agent efficacy. In order to completely leverage the droplet geometry, it is critically important to maintain spherical symmetry throughout the test. This can only occur if the diffusive residence times (i.e., mass (τ_m) and thermal (τ_k) are much lower than the buoyancy-controlled residence time (τ_b). Using the droplet diameter (D) as the characteristic length the expressions for the ratio of these two characteristic times to the buoyancy controlled residence time are

$$\frac{\tau_k}{\tau_b} = \frac{\sqrt{g\,D^3}}{\alpha_g} \tag{6}$$

and

$$\frac{\tau_m}{\tau_b} = \frac{\sqrt{g\,D^3}}{\mathcal{D}_g} \tag{7}$$

where α_g and $\mathcal{D}_g$ are the thermal and mass diffusivies of the gas phase. In order to justify neglecting buoyant effects the above ratios must be much lower than unity. This is only accomplished by changing at least one of the three independent variables, droplet diameter, pressure or gravity level (or some combination of the three).

Experiments in 1-g environments, performed in pressures of 1 atmosphere, require droplet diameters substantially smaller than 1 mm. This makes key diagnostics impractical since the image resolution begins to approach the dimensions of the distances being measured (e.g., flame standoffs, droplet regression, thin filament pyrometry). Also, the present experiment requires finite and measurable extinction droplet diameters (and a period of near quasi-steady burning prior to extinction) in order to quantify the influence of finite rate chemistry. The droplet diameters required to minimize buoyancy effects are small enough that extinction droplet diameters would either not be practically measurable or, more likely, not even exist.

Since diffusivities are inversely proportional to pressure the residence time ratios could alternatively be reduced by reducing test pressures. Chung and Law (1986) used this approach to measure extinction droplet diameters and from that determine single step chemical kinetic constants for decane in normal gravity. The range of oxygen concentrations and pressures was, however, very limited. Studying such a small range of droplet diameters, pressures and oxygen concentrations would severely limit the ability to achieve the stated objectives of the present study. Furthermore, Easton (1998) showed that the conditions that yielded finite extinction diameters in the work of Chung and Law (1986) burned to completion (no flame extinction) in microgravity. The author attributed this to a small residual buoyant-flow that is large enough in the vicinity of the flame to influence the extinction process (Struk et al., 1997).

The need for extended duration microgravity facilities is predicated on the fact that the burn-to-completion time for large droplets is longer than the time available in the ground-based facilities. Typically the droplet life-time (τ_l) can be estimated from the initial droplet size (D_0) and the average burning rate constant (k) as $\tau_l = \frac{D_0^2}{k}$. The values of τ_l for n-heptane, and methanol droplets burning in air at one atmospheric pressure range from 10 to 30 s for initial droplet diameters in the range 3 to 5 mm assuming an average burning rate constant of 0.8 mm^2/s. Moreover, high fidelity experiments demand additional microgravity time for droplet deployment, droplet quiescence, and ignition. Experiments involving radiative extinction require that the droplets be ignited in microgravity. Such experimental requirements also lead us to employ larger droplets, which in turn necessitates long-duration microgravity facilities. Both Dietrich et al. (2005) and

Easton (1998) studied extinction of single droplets in drop towers. Dietrich et al. (2005) used the Japan Microgravity Center 10 s drop tower, a facility no longer available, and even then could only study a limited parameter space because of the limited microgravity time. Therefore, the only facility which will enable data of sufficient quality over a wide parameter space is the microgravity environment available in extended-duration microgravity facilities (i.e. Space Shuttle or ISS).

References

(2003). Assessment of directions in microgravity and physical sciences research at nasa. National Academy Press.

Ackerman, M. and Williams, F. A. (2005). A simplified model for droplet combustion in a slow convective flow. *Combustion and Flame*, to appear.

Ackerman, M. D., Colantonio, R. O., Crouch, R. K., Dryer, F. L., Haggard, J. B., Linteris, G. T., Marchese, A. J., Nayagam, V., Voss, J. E., and Williams, F. A. (2003). A treatment of measurements of heptane droplet combustion aboard msl-1. TM 2003-212553, National Aeronautics and Space Adminimstration.

Aharon, I. and Shaw, B. D. (1998). On the roles of thermal diffusion and distinct binary coefficients in modeling droplet flame locations in microgravity. *Microgravity Science and Technology*, X/2:75–85.

Avedisian, C. T. (2000). Recent advances in soot formation from spherical droplet flames at atmospheric pressure. *Journal of Propulsion and Power*, 16(4):628–635.

Blake, T. R. (2002). Low reynolds number combustion of a spherical carbon particle. *Combustion and Flame*, 129:87–111.

Blake, T. R. and Libby, P. A. (1991). Combustion of a spherical carbon particle in slow viscous flow. *Combustion and Flame*, 86:147–159.

Chao, B. H., Law, C. K., and T'ien, J. S. (1990). Structure and extinction of diffusion flames with flame radiation. *Proceedings of the Combustion Institute*, 23:523–531.

Chaos, M., Kazakov, A., Zhao, Z., and Dryer, F. L. (2005a). High temperature compact mechanism development for large alkanes: n-heptane and iso-octane mixtures. to be published.

Chaos, M., Kazakov, A., Zhao, Z., Dryer, F. L., and Zeppieri, S. P. (2005b). High temperature compact mechanism development for large alkanes: n-hexadecane. In *6th International Conference on Chemical Kinetics*, page Poster C14, Gaithersburg, MD.

Cheatham, S. and Matalon, M. (1996). Near-limit oscillations of spherical diffusion flames. *AIAA Journal*, 34:1403–1409.

Chernovsky, M. K., Atreya, A., and Sacksteder, K. R. (2005). Effect of enhanced CO_2 concentration on radiative properties of unsteady spherical diffusion flames in microgravity. Joint Meeting of the US Sections of the Combustion Institute Poster Session.

Chiu, H. H. (2000). Advances and challenges in droplet and spray combustion: I. toward a unified theory of droplet aerothermochemistry. *Progress in Energy and Combustion Science*, 26:381–416.

Cho, S. Y., Yetter, R. A., and Dryer, F. L. (1992). A computer model for one-dimensional mass and energy transport in and around chemically reacting particles, including complex gas-phase chemistry, multicomponent molecular diffusion, surface evaporation, and heterogeneous reaction. *Journal of Computational Physics*, 102:160–179.

Choi, M. Y. and Dryer, F. L. (2001). Microgravity droplet combustion. In Ross, H. D., editor, *Microgravity Combustion: Fire in Free Fall*, Combustion Treatise, chapter 4, pages 183–297. Academic Press.

Choi, M. Y., Dryer, F. L., Haggard, J. B., and Brace, M. H. (1989). Some further observations on micro-gravity droplet combustion in the nasa-lewis drop tower facilities: A digital processing technique for droplet burning data. In Wang, T. G., editor, *Drops and Bubbles Third International Colloquium*, volume 197, pages 338–361. American Institute of Physics.

Choi, M. Y., Dryer, F. L., and Jr., J. B. H. (1990). Observations on a slow burning regime for hydrocarbon droplets: n-heptane/air results. *Proceedings of the Combustion Institute*, 23:1597–1605.

Choi, M. Y. and Lee, K. O. (1996). Investigation of sooting in microgravity droplet combustion. *Proceedings of the Combustion Institute*, 26:1243–1249.

Chung, S. H. and Law, C. K. (1986). An experimental study of droplet extinction in the absence of external convection. *Combustion and Flame*, 64:237–241.

Colantonio, R. and Nayagam, V. (1997). In *Proceedings of the Central States Section of the Combustion Institute*.

Dakhlia, R. B., Giovangigli, V., and Rosner, D. E. (2002). Soret effects in laminar counterflow spray diffusion flames. *Combustion Theory and Modeling*, 6:1–17.

Dietrich, D. L., Haggard, J. B., Dryer, F. L., Nayagam, V., Shaw, B. D., and Williams, F. A. (1996). Droplet combustion experiments in spacelab. *Proceedings of the Combustion Institute*, 26:1201–1207.

Dietrich, D. L., Struk, P. M., Ikegami, M., and Xu, G. (2005). Single droplet combustion of decane in microgravity: Experiments and numerical modeling. *Combustion Theory and Modeling*, to appear.

Dwyer, H. A. and Sanders, B. R. (1986). A detailed study of burning fuel droplets. *Proceedings of the Combustion Institute*, 21:633–639.

Dwyer, H. A., Shringi, D., and Shaw, B. D. (2004). A simulation of a fiber-supported droplet. *Computational Fluid Dynamics Journal*, 13:357–368.

Easton, J. W. (1998). Large diameter, radiative extinction experiments with decane droplets in microgravity. Master's thesis, Case Western Reserve University, Cleveland, Ohio 44106.

Faeth, G. M. (1977). Current status of droplet and liquid combustion. *Progress in Energy and Combustion Science*, 3:191–224.

Fendell, F. E. (1972). Asymptotic analysis of premixed burning with large activation-energy. *Journal of Fluid Mechanics*, 56:81 –.

Fendell, F. E., Sprankle, M. L., and Dodson, D. S. (1966). Thin-flame theory for a fuel droplet in a slow viscous flow. *Journal of Fluid Mechanics*, 26:268–280.

Friedman, R. (1998). Fire safety in extraterrestrial environments. TM 1998-207417, NASA.

Friedman, R. (1999). Fire safety in low-gravity spacecraft. TM 1999-209285, NASA.

Friedman, R. and Ross, H. D. (2001). *Mircogravity Combustion: Fire in Free Fall*, chapter Combustion Technology and Fire Safety for Human-crew Space Missions, pages 525–562. Academic Press.

Friedman, R. and Urban, D. L. (2000). Progress in fire detection and suppression technology for future space missions. TM 2000-210337, NASA.

Godsave, G. A. E. (1952). Studies of the combustion of drops in a fuel spray - the burning of single drops of fuel. *Proceedings of the Combustion Institute*, 4:818–830.

Gogos, G. and Ayyaswamy, P. S. (1988). A model for the evaporation of a slowly moving droplet. *Combustion and Flame*, 74:111–129.

Gogos, G., Sadhal, S., Ayyaswamy, P., and Sundarajan, T. (1986). *Journal of Fluid Mechanics*, 171:121.

Gokalp, I., Chauveau, C., Richard, J. R., Kramer, M., and Leuckel, W. (1988). Observations on the low temperature vaporization and envelope or wake flame burning of n-heptane droplets at reduced gravity during parabolic flights. *Proceedings of the Combustion Institute*, 22:2027–2035.

Goldsmith, M. (1956). Experiments on the burning of single drops of fuel. *Jet Propulsion*, 26:172–178.

Hall, A. R. and Diederichsen, J. (1953). An experimental study of the burning of single drops of fuel in air at pressures up to twenty atmospheres. *Proceedings of the Combustion Institute*, 4:837–846.

Hall, R. J. (1988). *Applied Optics*, 27:809–811.

Hamins, A., Trees, D., Seshadri, K., and Chelliah, H. K. (1994). Extinction of nonpremixed flames with halogenated fire suppressants. *Combustion and Flame*, 99:221 – 230.

Held, T. J., Marchese, A. J., and Dryer, F. L. (1997). A semi-empirical reaction mechanism for n-heptane oxidation and pyrolysis. *Combustion Science and Technology*, 123:107.

Hicks, M. C., Kaib, N., Easton, J., Nayagam, V., and Williams, F. A. (2003). Radiative heat loss measurements during microgravity droplet combustion in a slow convective flow. In *Proceedings of the Third Joint Meeting of the U.S. Sections of the Combustion Institute*, Chicago, IL. The Combustion Institute.

Honda, L. K. and Ronney, P. D. (1998). Effect of ambient atmosphere on flame spread at microgravity. *Combustion Science and Technology*, 133:267 – 291.

Jog, M. A., Ayyaswamy, P. S., and Cohen, I. M. (1996). *Journal of Fluid Mechanics*, 307:135.

Kassoy, D. R. and Williams, F. A. (1968). Variable property effects on liquid droplet combustion. *AIAA Journal*, 6:1961–1965.

Katta, V. R., Takahashi, F., and Linteris, G. T. (2004). Suppression of cup-burner flames using carbon dioxide in microgravity. *Combustion and Flame*, 137:506–522.

Kazakov, A., Conley, J., and Dryer, F. L. (2003). Detailed modeling of an isolated, ethanol droplet combustion under microgravity conditions. *Combustion and Flame*, 134(4):301–314.

Krishnamurthy, L., Williams, F. A., and Seshadri, K. (1976). Asymptotic theory of diffusion-flame extinction in stagnation-point boundary-layer. *Combustion and Flame*, 26:363 – 377.

Kroenlein, K. G., Kazakov, A., and Dryer, F. L. (2004). Isolated liquid droplet combustion: Inhibition and extinction studies. In *Conference-Workshop on Strategic Research to Enable NASA's Exploration Missions*, page Poster, Cleveland, OH. NASA.

Kroenlein, K. G., Kazakov, A., and Dryer, F. L. (2005). Reduced order models for droplet evaporation with internal circulation. In *Joint U.S. Sectional Meeting of the Combustion Institute*, page Paper D35, Drexel University, Philadelphia, PA. The Combustion Institute.

Law, C. K. (1975). Asymptotic theory for ignition and extinction in droplet burning. *Combustion and Flame*, 24:89–98.

Law, C. K. (1982). Recent advances in droplet vaporization and combustion. *Progress in Energy and Combustion Science*, 8:171–201.

Lee, J., Tomboulides, A. G., Orszag, S. A., Yetter, R. A., and Dryer, F. L. (1997). Transient two-dimensional chemically reactive flow model: Fuel particle combustion in a non-quiescent environment. *Proceedings of the Combustion Institute*, 26:3059.

Lee, K., Manzello, S., and Choi, M. (1998). *Combustion Science and Technology*, 132:139–156.

Li, J., Dryer, F. L., and Kazakov, A. (2005). Chemical kinetics of ethanol oxidation. In *2nd European Combustion Workshop*, pages Poster R15–019, Louvain-la-Neuve, Belgium.

Li, J., Zhao, Z., Kazakov, A., and Dryer, F. L. (2004a). Comprehensive kinetic mechanisms for c1 species combustion. In *30th International Symposium on Combustion*, pages Poster 1F1–04, Chicago, IL. The Combustion Institute.

Li, J., Zhao, Z., Kazakov, A., and Dryer, F. L. (2004b). An updated comprehensive kinetic model of hydrogen combustion. *International Journal of Chemical Kinetics*, 36:566.

Linan, A. (1974). The asymptotic structure of counterflow diffusion flames for large activation energies. *Acta Astronautica*, 1:1007–1039.

Manzello, S. L., Choi, M. Y., Kazakhov, A., Dryer, F. L., Dobashi, R., and Hirano, T. (2001). Sooting behavior of large droplets in the jamic facility. *Proceedings of the Combustion Institute*, 28:1079–1086.

Marchese, A. J. and Dryer, F. L. (1996a). The effect of liquid mass transport on the combustion and extinction of bicomponent droplets of methanol and water. *Combustion and Flame*, 105:104–122.

Marchese, A. J. and Dryer, F. L. (1996b). Microgravity combustion of methanol and methanol/water droplets: Drop tower experiments and model predictions. *Proceedings of the Combustion Institute*, 26:1209–1217.

Marchese, A. J. and Dryer, F. L. (1997a). *Combustion Science and Technology*, 124:371–402.

Marchese, A. J. and Dryer, F. L. (1997b). The effect of non-luminous thermal radiation in microgravity droplet combustion. *Combustion Science and Technology*, 124:373.

Marchese, A. J., Dryer, F. L., and Colantonio, R. O. (1999a). Radiative effects in space-based methanol/water droplet combustion experiments. *Proceedings of the Combustion Institute*, 27:2627.

Marchese, A. J., Dryer, F. L., and Nayagam, V. (1999b). Numerical modeling of isolated n-alkane droplet flames: Initial comparisons with ground and sace-based microgravity experiments. *Combustion and Flame*, 116:432–459.

Marchese, A. J., Dryer, F. L., Nayagam, V., and Colantonio, R. O. (1996). Hydroxyl radical chemiluminescence imaging and the structure of microgravity droplet flames. *Proceedings of the Combustion Institute*, 26:1219–1226.

Mehl, M., Cuoci, A., Faravelli, T., Ranzi, E., Kazakov, A., Dryer, F. L., Yozgatligil, A., Park, S. H., and Choi, M. Y. (2005). Combustion of ethanol fuel droplets in microgravity conditions. In *Proceedings of the 20th ILASS - Europe Meeting*, page Invited paper, Orleans, France.

Mills, K. and Matalon, M. (1998). Extinction of spherical diffusion flames in the presence of radiant loss. *Proceedings of the Combustion Institute*, 27:2535–2541.

Nayagam, V., Haggard, J. B., Colantonio, R. O., Marchese, A. J., Dryer, F. L., Zhang, B. L., and Williams, F. A. (1998). Microgravity n-heptane droplet combustion in oxygen-helium mixtures at atmospheric pressure. *AIAA Journal*, 36(8):1369–1378.

Nayagam, V., Hicks, M. C., Ackermann, M., Haggard, J. B., and Williams, F. A. (2003). Droplet combustion in a slow convective flow. In *Seventh International Workshop on Microgravity Combustion and Chemically Reacting Systems*, number CP-2003-212376, pages 157–160. NASA.

Nayagam, V. and Williams, F. (2000). Diffusion-flame extinction for a spinning fuel disk in an oxidizer counterflow. *Proceedings of the Combustion Institute*, 28:2875 – 2881.

Okajima, S. and Kumagai, S. (1974). Further investigations of combustion of free droplets in a freely falling chamber including moving droplets. *Proceedings of the Combustion Institute*, 15:401–407.

Okajima, S. and Kumagai, S. (1982). Experimental studies on combustion of fuel droplets in flowing air under zero- and high-gravity conditions. *Proceedings of the Combustion Institute*, 19:1021–1027.

Olson, S. L., Ferkul, P. V., and T'ien, J. S. (1988). Near-limit flame spread over a thin solid fuel in microgravity. *Proceedings of the Combustion Institute*, 22:1213–1222.

Opfell, J. (1985). Fire detection and fire suppression trade study. Technical Report 85-22472, Rev. 1, Allied-Signal Aerospace Co.

Panzarella, L. N. and Lewis, P. (1990). Crew lock/hyperbaric chamber fds fire suppressant selection trade study. Memorandum A96-J753-STN-M-LP-900070, McDonnell Douglas (Houston).

Pope, D. N. and Gogos, G. (2005). Numerical simulation of fuel droplet extinction due to forced convection. *Combustion and Flame*, 142:89–106.

Reuther, J. J. (1985). Definition of experiments to investigate fire suppressants in microgravity. NASA CR- 185295, NASA.

Rosner, D. E., Israel, R. S., and LaMantia, B. (2000). Heavy species ludwig-soret transport effects in air-breathing combustion. *Combustion and Flame*, 123:547–560.

Shaw, B. D. (2005). Theory of spherically symmetrical droplet combustion with gas-phase fuel pyrolysis. *Combustion Science and Technology*, 177:1151–1166.

Shaw, B. D., Clark, B. D., and Wang, D. F. (2001). Spacelab experiments on combustion of heptane-hexadecane droplets. *AIAA Journal*, 39:2327–2355.

Shringi, D., Dwyer, H. A., and Shaw, B. D. (2005). Effects of supporting rods on fuel droplet heating and vaporization with surface tension effects. In *Fall Meeting of the Western States Section of the Combustion Institute*, number 04F-53, Stanford, CA. The Combustion Institute.

Sirignano, W. A. (1993). Fluid dynamics of sprays - 1992 freeman scholar lecture. *ASME Journal of Fluids Engineering*, 115:346–378.

Sirignano, W. A. (1999). *Fluid dynamics and transport of droplets and sprays*. Cambridge University Press.

Spalding, D. B. (1952). The combustion of liquid fuels. *Proceedings of the Combustion Institute*, 4:847–864.

Spalding, D. B. (1953). Experiments on the burning and extinction of liquid fuel spheres. *Fuel*, 32:169–185.

Struk, P. M., Ackerman, M., Nayagam, V., and Dietrich, D. L. (1998). On calculating burning rates during fiber supported droplet combustion. *Microgravity Science and Technology*, XI/4:144–151.

Struk, P. M., T'ien, J. S., Dietrich, D. L., and d B Lenhert (1997). Experimental studies of flame shape around droplets in different buoyant environments. 35th Aerospace Sciences Meeting and Exhibit AIAA-97-1001, American Institute of Aeronautics and Astronautics.

Takahashi, F., Linteris, G. T., and Katta, V. R. (2004). Fire suppression in low gravity using a cup burner. Conference-Workshop on Strategic Research to Enable NASA's Exploration Missions.

T'ien, J. S. (1990). The possibility of a reversal of material flammability ranking from normal gravity to microgravity. *Combustion and Flame*, 80:355 – 357.

Urban, B. D., Kroenlein, K., Kazakov, A., Dryer, F. L., Yozgatligil, A., Choi, M. Y., Manzello, S. L., Lee, K. O., and Dobashi, R. (2004). Sooting behavior of ethanol droplet combustion at elevated pressures under microgravity conditions. *Microgravity Science and Technology*, XV/3.

Warnatz, J., Maas, U., and Dibble, R. W. (1996). *Combustion: Physical and Chemical Fundamentals, Modeling and Simulation, Experiments, Pollutant Formation*. Springer-Verlag, Berlin.

Wei, J. B. and Shaw, B. D. (2005). in preparation.

Williams, A. (1973). Combustion of droplets of liquid fuels: A review. *Combustion and Flame*, 21:1–31.

Williams, B. A. (2001). Sensitivity of calculated extinction strain rate to molecular transport formulation in nonpremixed counterflow flames. *Combustion and Flame*, 124:330–333.

Williams, F. A. (1974). A unified view of fire suppression. *Journal of Fire and Flammability*, 5:54–63.

Williams, F. A. (1981). Droplet burning. In Cochran, T. H., editor, *Progress in Astronautics and Aeronautics*, volume 73, chapter 2, pages 31–60. American Institute of Aeronautics and Astronautics.

Wise, H. and Agoston, G. A. (1958). Burning of liquid droplets. In *Advances in Chemistry*, 20, pages 116–135. American Chemical Society, Washington, D.C.

Wu, M. S. and Ruff, G. A. (2003). Numerical simultation of co2 dispersion in the combustion integrated rack (cir). In *Seventh International Workshop on Microgravity Combustion and Reacting Systems*. National Aeronautics and Space Administration.

Wu, X., Law, C. K., and Fernandez-Pello, A. C. (1982). A unified criterion for the convective extinction of fuel particles. *Combustion and Flame*, 44:113–124.

Yozgatligil, A. (2005). PhD thesis, Drexel University.

Yozgatligil, A., Park, S. H., and Choi, M. Y. (2005). The effect of inert substitution on ethanol droplet combustion in microgravity. In *Proceedings of the 4th Joint Meeting of the U.S. Sections of the Combustion Institute*, Philadelphia, PA. The Combustion Institute.

Yozgatligil, A., Park, S. H., Choi, M. Y., Kazakov, A., and Dryer, F. L. (2004a). Burning and sooting behavior of ethanol droplet combustion under microgravity conditions. In *30th International Symposium on Combustion*, pages Poster 1F3–02, Chicago, IL. The Combustion Institute.

Yozgatligil, A., Park, S. H., Choi, M. Y., Kazakov, A., and Dryer, F. L. (2004b). Burning and sooting behavior of ethanol droplet combustion under microgravity conditions. *Combustion Science and Technology*, 176:1985–1999.

Zhang, B. L. and Williams, F. A. (1997). Theoretical sudies of methanol droplet combustion based on results from the usml-2 mission. *Acta Astronautica*, 40:829–835.

Zhang, B. L. and Williams, F. A. (1998). Effects of the lewis number of water vapor on the combustion and extinction of methanol droplets. *Combustion and Flame*, 112:113–120.

Zhao, Z., Li, J., Kazakov, A., and Dryer, F. L. (2005). Burning velocities and a high temperature skeletal kinetic model for n-decane. *Combustion Science and Technology*, 177:89–106.

Zhao, Z., Li, J., Kazakov, A., Dryer, F. L., and Zeppieri, S. P. (2004). Burning velocities and a high temperature skeletal kinetic model for n-decane oxidation. In *30th International Symposium on Combustion*, pages Poster 4I6–05, Chicago, IL. The Combustion Institute.

A Previous Microgravity Droplet Combustion Experiments

The present project builds on extensive ground-based droplet combustion experiments conducted in the drop-towers at NASA Glenn Research Center as a part of the previously planned flight experiments (DCE-2, BCDCE, SDCE, and DDCE) as well as three flight experiments conducted onboard the space shuttle, namely FSDC (Fiber Supported Droplet Combustion Experiment), DCE (Droplet Combustion Experiment), and FSDC-2. Though these experiments were primarily focused on the fundamental aspects of droplet combustion, the fundamentals addressed by these experiments are essential to the fundamentals that impact fire sensing and suppression technologies applicable to space exploration environments. In the following, the relevance of these experiments to the proposed effort is described briefly.

A.1 Ground-Based Low Gravity Experiments

As a part of FLEX Phase A activities we built and tested a drop-tower rig for use in the 5-second Zero Gravity Facility at the GRC. We have conducted several droplet combustion tests to resolve the various feasibility issues associated with FLEX. In the experiments, the droplet is suspended on a quartz fiber and ignited using a hot-wire igniter. Gas mixing is done via partial pressure filling from premixed gas bottles. The rig is capable of generating accurate forced flow velocities in the range 0 to 3 cm/s. The droplet is deposited on a fiber supported by a fixture and, along with cameras and radiometers; this fixture is translated at precisely controlled speeds using a stepper motor and lead-screw mechanism. This technique will allow us to examine the effects of steady and accelerated convective flow on suppression.

During DDCE hardware development phase we have proven the feasibility of hot-wire ignition techniques for both methanol and heptane fuels under microgravity in a variety of environmental conditions (Marchese and Dryer, 1996b), the use of thin Si-C fibers as fiber support, $OH*$-chemiluminescence imaging (Marchese et al., 1996), measurement of radiative heat loss using radiometers (Colantonio and Nayagam, 1997), the interpretation of radiometer measurements (Kazakov et al., 2003) and all the related data analysis techniques (automated PC-based image analysis system) involved in droplet combustion experiments. Recent experiments and numerical modeling efforts also illustrate the effects of different suppressants and the need for larger droplets and longer microgravity times to fully investigate extinction phenomena (e.g. Yozgatligil, 2005).

As part of the experiments in support of the Sooting and Radiation Effects in Droplet Combustion (SEDC), many interesting behaviors of diffusion flame characteristics were uncovered. Several important experimental tools that were developed and tested as part of this program include full-field light extinction (Choi and Lee, 1996), two-wavelength pyrometry (Lee, 1996), and thermophoretic sampling of flame-generated particulates (Manzello et al., 2001). These experiments demonstrated that sooting propensities of fuels in microgravity conditions is significantly higher than those that are encountered at the same environmental conditions under normal-gravity.

For example, even a lightly sooting fuel such as n-heptane (characterization based on observation of sooting behavior of n-heptane in normal gravity conditions) produced maximum soot volume fractions as high as 60 ppm. The accumulated soot will have profound effects on the flame structure by reducing the temperature, enhancing the radiative emission that may lead to premature flame extinction, and reductions in the burning rate. These influences must be investigated to gain a more complete understanding of the influence of environmental conditions on the burning and extinction behavior of fuels. Variation in the oxygen concentration, reduction in the ambient pressure, and the substitution of inerts will exert varying influences on the overall sooting behavior and thus the burning behavior.

While the numerical modeling efforts continue to progress toward including particulate sooting effects, the work has already predicted that that carbon dioxide substitution for nitrogen in the burning of large carbon number hydrocarbon liquid droplets leads to a significant effects partly through increased heat capacity within the gaseous diffusion flame, but mostly because of modifcations in spectral radiative coupling in the gas phase. Effects of sooting and slow gas-phase/droplet convection remain to be considered in future numerical modeling studies. The work also shows that the modeling methodologies can be developed to evaluate the effects of chemical inhibitors in the liquid and gas phases.

The BCDCE program has produced results that are of relevance to the proposed FLEX program. Specifically, BCDCE expertise can contribute to FLEX by quantifying fiber influences analytically and computationally) and interpreting data in terms of influences of droplet shapes, internal flows, liquid mixing rates and product dissolution. The BCDCE research has also developed a 3-d computational model of a droplet on a fiber, including capillary flows induced by the fiber. A cross flow can be modeled, which is relevant to a droplet anchored on a moving fiber. However, the computational model presently covers only vaporizing droplets. It is planned to extend this model to include combustion, depending on funding levels. UC Davis also has a working drop rig that can be used for experiments up to about 10 atm.

A.2 Fiber Supported Droplet Combustion Experiment (FSDC)

FSDC was the first droplet combustion experiment conducted in space. In this Glovebox experiment, in a procedure somewhat similar to the current project, a shuttle crew member deposited a measured amount of fuel droplet (initial diameters varied between 2 and 5 mm) on a silicon-carbide fiber (80 μm diameter) and ignited them in cabin air environment using a hot-wire igniter. The results of these experiments are summarized in Dietrich et al. (1996) and Shaw et al., (2001a, 2001b). This experiment, for the first time, produced the radiative extinction of large methanol droplets in a quiescent, microgravity environment. In the forced convective part of FSDC-1 experiments, droplets were burned initially in a quiescent environment and then forced convective flow (generated by a fan) was turned on so that both spherically symmetric and convective droplet burning were observed. The dynamics of flame response were also documented. The convective velocities in these experiments were of the order of 10 cm/s and radiative extinctions were not observed for the methanol and heptane/hexadecane fuel droplets studied.

A.3 Fiber Supported Droplet Combustion Experiment - 2 (FSDC-2)

FSDC-2 experiments were conducted during the MSL-1 mission (STS-94) of the space shuttle Columbia in April 1997. In these experiments radiative extinction for ethanol, methanol, n-heptane, and n-decane fuels were observed in a quiescent environment. Flow effects on sooting and non-sooting were also investigated in the intermediate Reynolds number regime $Re \sim O(100)$ (Colantonio et al. 1998). The FSDC experiments clearly demonstrated the feasibility of performing fiber supported droplet combustion experiments as well as the experimental technique of extracting flame position as function of time from the Si-C fiber radiation. These experiments strongly support the feasibility of the proposed experiments. Results from the FSDC-2 experiments are described by Shaw et al. (2001a).

A.4 Droplet Combustion Experiment (DCE)

The Droplet Combustion Experiment is a high fidelity experiment conducted inside a pressure vessel onboard the Spacelab during MSL-1 mission. Free floated, n-heptane droplets were burned in

oxygen/helium environments at three different pressures (0.25, 0.5, and 1 atm.). At low oxygen concentrations and at large initial droplet sizes radiative extinction was observed (Nayagam et al., 1998). All the radiative extinctions observed during these experiments were essentially in a quiescent environment (droplet drift velocities $\sim$ 2 mm/s) and the flames were spherical. Extinction occurs suddenly and with no obvious preferential starting point (within the time resolution of observation 1/30 sec). At high oxygen concentrations, when the drift velocities of the order a few mm/s were present, only 'diffusive extinctions' were observed. Diffusive extinction of this nature, however, was hardly perturbed by the slow convective effects. One of the lessons learned during these experiments relevant to the proposed study is that it is very difficult, if not impossible, to control the droplet/gas relative velocities in a free floated droplet combustion experiment. This fact has led us to use the small Si-C fiber to support the droplet and produce precisely controllable velocities by translating the tethered droplet in a quiescent environment.

A.5 Ground-based studies of Soot Formation/Destruction

Controlling the degree of sooting is important for developing an accurate understanding of its influence on droplet burning, flame dynamics, and flame extinction. All of the independent experimental variables (initial droplet diameter, diluents and suppressants, oxygen mole fraction, pressure, fuel type, convection) to be used in the FLEX experiments have been demonstrated in previous microgravity experiments to strongly influence the degree of sooting and droplet burning behavior which will thereby affect flame extinction. The background section on droplet combustion clearly showed how initial droplet size and forced convective flow velocity influence sooting behavior. The FLEX team has conducted additional experiments to show how different inert gases (or suppressant gases) influence sooting behavior.

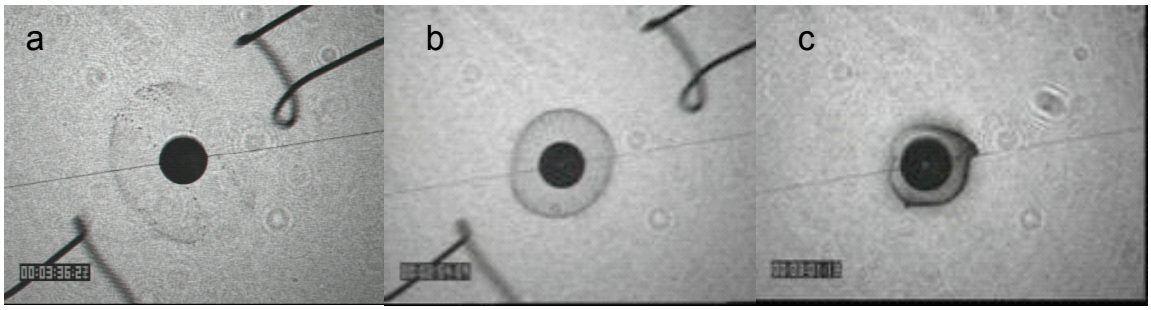

Figure 9: Laser backlit images for ethanol droplets burning at 2.4 atmospheres and 30% oxygen concentration in a) He b) N_2 c) Ar.

Figure 9 displays the laser-backlit image of the ethanol droplets burning in 30% oxygen/helium, 30% oxygen/nitrogen, and 30% oxygen/argon environments at 2.4 atmospheres (Yozgatligil et al., 2005). Although locations vary, distinct sootshells are observed for all three inert cases. For

Table 13: Residence time (τ_{res}) and flame temperature (T_f) for ethanol droplets burning in ambients with different diluent gases and an oxygen mole fraction of 0.30.

Ambient	$d\ (mm)$	$k\ (mm^2/s)$	$\tau_{res}\ (s)$	$T_f\ (K)$
Ar	1.94	0.55	0.27	2344
N_2	2.02	0.56	0.25	2105
He	1.99	0.96	0.12	1809

the oxygen/argon inert case, the sootshell is significantly more opaque (corresponding to higher soot concentration and greater amount of laser attenuation) than the oxygen/nitrogen and oxygen/helium inert cases.

The residence times of the fuel vapor within the region bounded by the droplet surface and the flame front were calculated and the results are summarized along with the burning rate and flame temperature measurements in Table 1 for the three inert cases. Residence times of ethanol fuel vapor in the oxygen/helium inert case is a factor of two lower than the oxygen/nitrogen and oxygen/argon inert cases. This is mainly due to the higher Stefan flux associated with increased burning rates in the oxygen/helium inert case. Since the residence time in both argon and nitrogen inert cases are very similar, the large difference in the soot yield is not caused by the influence of residence time. Comparisons of the flame temperatures indicate that the oxygen/argon inert case exhibits the highest temperature, followed by the oxygen/nitrogen and oxygen/helium cases, respectively. Therefore, the combination of higher fuel vapor residence time and higher temperature accounts for the dramatic increase in sooting for the oxygen/argon case compared to the oxygen/helium case.

Figure 10 displays the laser-backlit view of ethanol droplets burning in 30% and 40% concentrations in nitrogen at 2.4 *atm* pressure (Yozgatligil et al., 2005). These experiments clearly demonstrate the strong dependence of sooting behavior of ethanol droplets on ambient pressure and oxygen concentration. As the oxygen concentration is increased, the sooting propensity (based on visual observation of the opacity of the sootshell) appears to vary in a non-monotonic fashion, first increasing and then decreasing with increasing oxygen concentration. The maximum soot volume fractions ($\{_{v,\,max}$) were also measured for these experiments. At 21% O_2 in N_2 , the maximum soot volume fraction is approximately 10 *ppm*, while at 30% O_2 in N_2 , the maximum soot volume fraction is approximately 17.5 *ppm*. As the oxygen concentration is increased, the maximum soot volume fraction decreased from 11 *ppm* at the 35% O_2 in N_2 to less than 5 *ppm* at the 45% O_2 in N_2 case.

Increases in the oxygen concentration result in smaller droplet flames and higher rates of burning which causes reductions in the fuel vapor transport time. Both of these effects will tend to reduce the time for soot formation and growth. At the same, increases in the oxygen concentration will produce higher flame temperatures which increase the rate of pyrolysis reactions leading to greater degree of soot precursor and soot formation. The non-monotonic behavior is believed to be caused by the competition between soot formation and soot oxidation. Numerical calculations also indicate that concentrations of soot precursors such as benzene display a non-monotonic behavior with oxygen concentration (Mehl et al., 2005).

In 1997, Lee et al. (1997) used ambient pressure reduction to control sooting in microgravity droplet combustion. Figure 11 displays the laser-backlit image at $t = 0.5\ sec$ after ignition for n-heptane droplets burning under 1.0 *atm*, 0.75 *atm*, 0.5 *atm* and 0.25 *atm*, respectively. As pressure is reduced, the attenuation of the laser intensity becomes less pronounced, and the well-defined

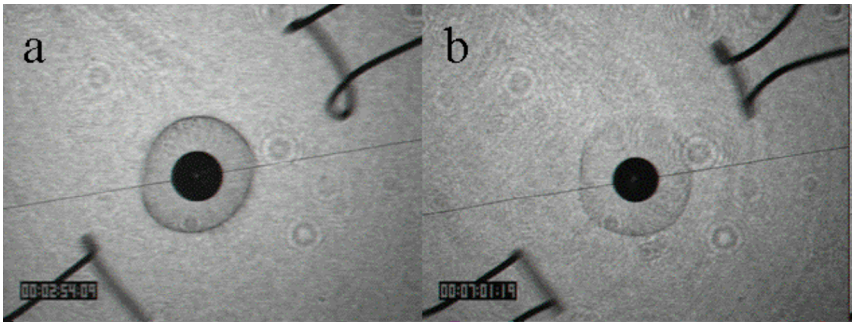

Figure 10: Ethanol droplets burning in O_2 /N_2 of a) 30%/70% and b) 40%/60% and an ambient pressure of 2.4 atm.

sootshell observed in the 1 atm experiment is clearly diminished at the 0.5 atm. It has also been observed in subsequent microgravity investigations that radiant loss rates associated with sooting should decrease with increasing dilution and decreasing pressure (Williams, 2001).

A.6 Ground-based studies of Soret Diffusion

Aharon and Shaw (1998) developed analytical models to describe transport of O_2 to droplet flames under quasisteady conditions, with a particular emphasis of evaluating Soret transport as well as multicomponent diffusion effects that occurs as a result of variations in binary diffusion coefficients. Their models predicted that Soret transport can oppose transport of O_2 to a reaction zone if the diluent has a small molecular weight relative to the molecular weight of O_2 , which is the case for He . Conversely, transport of O_2 to a reaction zone is enhanced via Soret effects if the diluent molecular weight is large relative to the molecular weight of O_2 , which is the case for SF_6 (or Xe). For a diluent such as N_2 , which has a molecular weight that is close to the molecular weight of O_2 , Soret effects are small. It was also shown that multicomponent diffusion effects can be important if significant differences between binary species diffusion coefficients are present. The relative influences of Soret transport and multicomponent diffusion effects on an effective O_2 diffusion coefficient, $\mathcal{D}_O$ are given in the following relationship.

$$\mathcal{D}_O = \beta\,\phi\,\mathcal{D}_{IO} \tag{8}$$

where β accounts for Soret transport, ϕ multicomponent diffusion (accounting for the presence of combustion-generated CO_2 and H_2O) and $\mathcal{D}_{IO}$ is the binary diffusion coefficient of O_2 in the diluent (e.g., He) (Aharon and Shaw, 1998). When $\beta > 1$, Soret transport enhances O_2 transport to flame zones, and when $\beta < 1$ Soret transport opposes O_2 transport to flame zones. These same conclusions also apply to ϕ, which accounts for differences between binary diffusion coefficients in a multicomponent gas mixture.

Shaw (2005) used the predictions of Aharon and Shaw (1998) to interpret experimental results

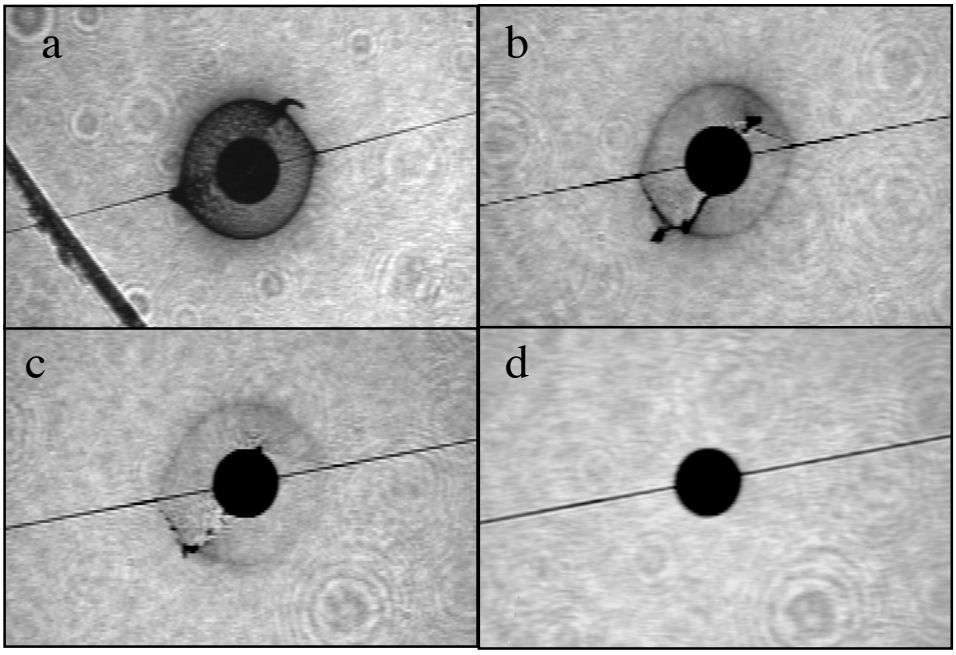

Figure 11: Heptane droplets burning in air at pressures of a) 1 atm, b) 0.75 atm, c) 0.5 atm, d) and 0.25 atm.

from reduced-gravity droplet combustion experiments in environments with He , N_2 , or Xe as diluents. The droplets, which were initially about $1\,mm$ in diameter, were composed of $C_{10}H_{22}/C_{16}H_{34}$ (decane/hexadecane) mixtures with initial $C_{16}H_{34}$ mass fractions of 0, 0.05 and 0.20. Individual fiber-supported droplets were burned at $0.1\ MPa$ with an ambient O_2 mole fraction of 0.21 for all diluents. The data showed strong variations in flame temperature with changes in the inert gas. The experiments with Xe appeared to have significantly higher flame temperatures than the experiments with either He or N_2 , which is consistent with the Le_O discussion earlier.

Figure 12 presents representative images from the experiments and clearly shows the influence of the inert gas on sooting behavior, flame brightness and relative flame sizes. When He was the diluent, there was not any visible sooting and flame diameters were relatively large. Xe produced the brightest and smallest flames, and N_2 produced intermediate results. Based on molecular weight considerations, using the SF_6 as a diluent will likely produce results similar to the Xe tests.

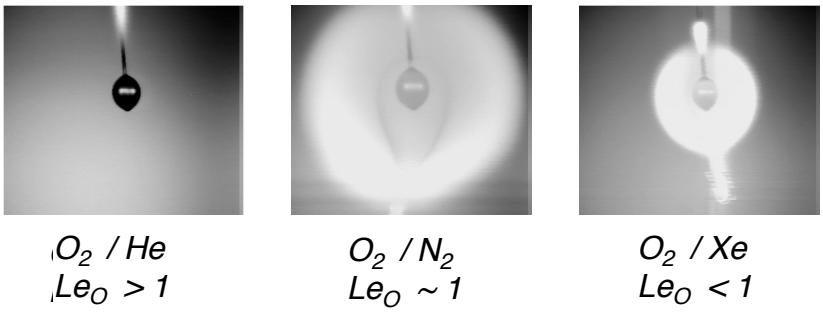

Figure 12: Images from Shaw (2005) for reduced-gravity combustion of decane/hexadecane droplets with different inert gases.

Figure 13 shows representative burning rate and flame standoff data from Shaw (2005). The influence of the inert gas is obvious from this figure. He produced the largest amount of gas-phase unsteadiness because transport of O_2 to the reaction zone was significantly inhibited.

Table 14 shows β, and ϕ values for various environments (Shaw, 2005) assuming that decane is the predominant fuel species in the gas phase. Also shown are $\mathcal{D}_{IO}$ and $\mathcal{D}_O$ values for $0.1\ MPa$ as well as the O_2 Lewis numbers that correspond to these diffusivities.

Table 14 shows that low molecular weight inerts (in this case, He) significantly oppose transport of oxygen to the flame zone via Soret effects ($\beta = 0.24$) and multicomponent diffusion effects ($\phi = 0.65$), while inerts that are similar to O_2 (in this case, N_2) do not play a significant role in terms of Soret effects ($\beta = 0.96$) or multicomponent diffusion ($\phi = 0.94$). In contrast, a high

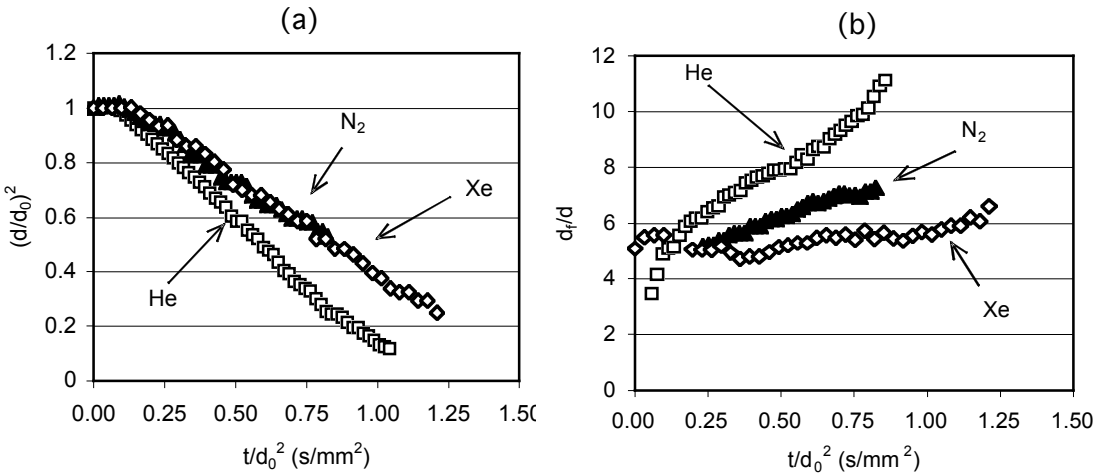

Figure 13: Data from Shaw (2005): (a) normalized droplet diameter histories; and (b) flame standoff ratios.

Table 14: Gas-phase oxygen transport data for different inert species in a 0.21 oxygen mole fraction ambient.

Inert	β	ϕ	$\mathcal{D}_{IO}$ (cm^2/s)	$\mathcal{D}_O$ (cm^2/s)	Le_O $(\mathcal{D}_{IO})$	Le_O $(\mathcal{D}_O)$
He	0.24	0.65	10.3	1.6	1.4	> 2.0
N_2	0.96	0.94	3.8	3.4	1.05	1.16
Xe	1.46	1.03	2.4	3.6	0.64	0.43

molecular weight inert (in this case, Xe) significantly promotes transport of oxygen to the flame zone from Soret effects ($\beta = 1.46$), though multicomponent diffusion is not significantly enhanced ($\phi = 1.03$). Based on these results, it is clear that varying the molecular weight of the inert component in the ambient over significant ranges strongly influences the contributions of Soret transport and multicomponent diffusion on transport of O_2 to flames.

Further drop tower experiments along these same lines have been performed by Wei and Shaw (2005). Reduced-gravity experiments involved burning individual propanol droplets that were initially about 1 mm in diameter. The environment was composed of an O_2 -inert mixture, where He , Ar, Xe and N_2 were used separately as inerts. The O_2 mole fraction in the environment was 0.21 or 0.50, and the pressure ranged from 0.03 MPa $-$ 1.0 MPa. Data from the experiments indicate that combustion characteristics depend significantly on the inert species. He produced larger and apparently cooler flames while Xe produced flames that were significantly smaller and hotter (for approximately the same initial droplet diameter). N_2 and Ar produced intermediate results. Extensions of these experiments to other fuels (methanol and heptane) and other diluents (CO2 and SF6) are presently being pursued.

The ground-based experiments described above were limited to smaller droplets ($\approx$ 1 mm in diameter or smaller) that can be burned to completion (or near completion) in drop towers. Larger droplets, e.g., up to 5 mm initially or larger, which have long burn times, cannot be studied using ground-based reduced-gravity facilities because of experiment time limitations, which means that influences of extended length and time scales relevant to spacecraft environments cannot be investigated unless space-based experiments are performed.

A.7 Summary

The analytical and numerical modeling work accompanying the above experimental efforts has guided the development of test matrices for the specific experiments as well as interpreted the data obtained from these efforts have significantly advanced understanding of the dynamics of droplet combustion, inclusive of the dynamics of flame position during droplet burning, including extinction processes, the effects of combustion product dissolution, multi-component vaporization, non-luminous radiation coupling, sooting, Soret transport, multicomponent diffusion, and slow convection on burning rate parameters, flame structure, and extinction, The sub-models developed for chemical kinetics in these studies have been extensively used in industry, particularly in the aircraft gas turbine development efforts at both GE aircraft and United Technologies Research Center. A bibliography of references that detail the specifics of these theoretical works and their comparisons with the above experiments are attached as Appendix